**Atmospheric
Chemistry
and Physics**

Organic nitrate and secondary organic aerosol yield from NO$_3$ oxidation of β-pinene evaluated using a gas-phase kinetics/aerosol partitioning model

J. L. Fry[1]**, A. Kiendler-Scharr**[2]**, A. W. Rollins**[1]**, P. J. Wooldridge**[1]**, S. S. Brown**[3]**, H. Fuchs**[3]**, W. Dubé**[3]**, A. Mensah**[2]**,
M. dal Maso[2]**, R. Tillmann**[2]**, H.-P. Dorn**[2]**, T. Brauers**[2]**, and R. C. Cohen**[1]

[1]Department of Chemistry, University of California, Berkeley, CA, USA
[2]ICG-2: Troposphäre, Forschungszentrum Jülich, 52425 Jülich, Germany
[3]Chemical Sciences Division, NOAA Earth System Research Laboratory, Boulder, CO, USA

Abstract. The yields of organic nitrates and of secondary organic aerosol (SOA) particle formation were measured for the reaction NO$_3$+β-pinene under dry and humid conditions in the atmosphere simulation chamber SAPHIR at Research Center Jülich. These experiments were conducted at low concentrations of NO$_3$ (NO$_3$+N$_2$O$_5$<10 ppb) and β-pinene (peak∼15 ppb), with no seed aerosol. SOA formation was observed to be prompt and substantial (∼50% mass yield under both dry conditions and at 60% RH), and highly correlated with organic nitrate formation. The observed gas/aerosol partitioning of organic nitrates can be simulated using an absorptive partitioning model to derive an estimated vapor pressure of the condensing nitrate species of p_{vap}∼5×10^{-6} Torr (6.67×10^{-4} Pa), which constrains speculation about the oxidation mechanism and chemical identity of the organic nitrate. Once formed the SOA in this system continues to evolve, resulting in measurable aerosol volume decrease with time. The observations of high aerosol yield from NO$_x$-dependent oxidation of monoterpenes provide an example of a significant *anthropogenic* source of SOA from *biogenic* hydrocarbon precursors. Estimates of the NO$_3$+β-pinene SOA source strength for California and the globe indicate that NO$_3$ reactions with monoterpenes are likely an important source (0.5–8% of the global total) of organic aerosol on regional and global scales.

1 Introduction

Organic material constitutes a major fraction (Kanakidou et al., 2005; Fuzzi et al., 2006; Zhang et al., 2007) of atmospheric aerosol particulate matter, which affects Earth's climate by absorbing and scattering solar radiation and altering the brightness and lifetime of clouds (Forster et al., 2007) and has been implicated in asthma, heart and lung disease, and mortality (Dockery and Pope, 1994; Pope et al., 1995; Alfaro-Moreno et al., 2007; Pope, 2007). Organic particles can be emitted directly to the atmosphere, for example by incomplete combustion or biomass burning, constituting primary organic aerosol (POA). They can also be formed in the atmosphere by gas-to-particle conversion of condensable organic compounds (Seinfeld and Pankow, 2003), constituting secondary organic aerosol (SOA). Recent studies indicate that SOA is a major fraction of total organic aerosol, up to 90% regionally (Turpin and Huntzicker, 1995; Kanakidou et al., 2005), with the source underestimated by 1–2 orders of magnitude in models (de Gouw et al., 2005; Heald et al., 2005; Volkamer et al., 2006; Goldstein and Galbally, 2007), indicating that the chemistry of atmospheric secondary organic aerosol (SOA) formation remains incompletely understood.

The three major atmospheric oxidants driving SOA formation from biogenic VOCs are OH, O$_3$, and the nitrate radical (NO$_3$). While O$_3$-initiated reactions occur at all times, reactions with OH radicals occur primarily during the day, because OH is photochemically produced, and reactions with NO$_3$ occur primarily during the night, because the nitrate radical photolyzes rapidly under visible radiation.

Table 1. Atmospheric oxidants and lifetime of β-pinene.

Oxidant	$k_{Ox+\beta-pinene}$ (cm^3 molecules^{-1}s^{-1})	Average [Ox] (molecules cm^{-3})	τ_{Ox}
O$_3$	1.5×10^{-17}	7×10^{11} (30 ppb) (24 h average)	26.5 hr
OH	7.89×10^{-11}	1×10^{6} (0.04 ppt) (12 h daytime average)	3.5 hr
NO$_3$	2.51×10^{-12}	2.4×10^{8} (10 ppt) (12 h nighttime average)	0.5 hr

Large NO$_3$-initiated aerosol formation from biogenic volatile organic compounds (VOCs) would provide one potential resolution to an apparent paradox noted in the SOA literature: while radiocarbon measurements indicate a large fraction of modern carbon in aerosol from urban ($\sim$50%) to remote areas (80–100%) (Schichtel et al., 2008), SOA plumes in both types of locations have been frequently observed to be correlated with anthropogenic sources (de Gouw et al., 2005; Quinn et al., 2006; Weber et al., 2007). This mechanism, if a significant SOA source, resolves the paradox by requiring both an *anthropogenic* oxidant and *biogenic* VOC to form aerosol.

In regions of high NO$_x$ (=NO+NO$_2$) and O$_3$, NO$_3$ builds up when photolysis is inefficient. As such, NO$_3$-initiated oxidation processes are expected to be important in nighttime or within-canopy atmospheric chemistry, especially downwind of urban areas or power plants. Although the role of NO$_3$ as a dominant sink for biogenic compounds was suggested in the early 1980s (Winer et al., 1984), most studies on the atmospheric oxidation of monoterpenes to date have focused on OH- and O$_3$-initiated oxidation, with only a few studying NO$_3$-initiated degradation of VOCs (Jay and Stieglitz, 1989; Atkinson, 1997; Berndt and Boge, 1997; Hoffmann et al., 1997; Wangberg et al., 1997; Hallquist et al., 1999; Calvert et al., 2000; Bonn and Moortgat, 2002; Spittler et al., 2006) or SOA formation (Hoffmann et al., 1997; Griffin et al., 1999a; Hallquist et al., 1999; Moldanova and Ljungstrom, 2000; Gong et al., 2005; Spittler et al., 2006; Ng et al., 2008). While O$_3$ is more abundant throughout the atmosphere, reaction rates of alkenes are faster with OH and NO$_3$, and NO$_3$ is much more abundant during the night than OH is during the day. This leads to atmospheric lifetimes to NO$_3$ oxidation being shorter than both OH and O$_3$ lifetimes at typical atmospheric concentrations for many VOCs (see Table 1 for the values for β-pinene). Recent field studies have shown evidence that NO$_3$ oxidation is a significant removal process for several alkenes in the atmosphere, even at sub-ppt daytime concentrations (Geyer et al., 2001, 2003; Kurtenbach et al., 2002; Aldener et al., 2006).

Here we describe measurements and kinetic modeling of gas- and aerosol-phase chemistry during SOA formation initiated by the NO$_3$+β-pinene reaction, under dry and humid conditions. We find that aerosol formation is correlated with organic nitrate formation, suggesting that this product channel is responsible for condensation and that ambient atmospheric aerosol formed via this mechanism should contain organic nitrate signatures.

2 Experimental

2.1 Atmosphere simulation chamber SAPHIR

All experiments were conducted in the atmospheric simulation chamber SAPHIR at Research Center Jülich. The SAPHIR chamber is designed for controlled studies of chemical systems under atmospheric conditions, and has recently been used to study e.g. the HCHO cross section, HONO photolysis, NO$_3$+aldehydes, O$_3$+alkenes, and NO$_2$ photolysis (Bohn et al., 2005; Rohrer et al., 2005; Bossmeyer et al., 2006; Brauers et al., 2007; Wegener et al., 2007). The chamber is a double-walled 120 μm thick FEP foil (DuPont) container of cylindrical shape with an effective volume of $\sim$270 m^3 (5 m diameter and 18 m length). The space between the two walls is flushed continuously with high-purity N$_2$ and the chamber interior is maintained at 0.3–0.45 Torr (40–60 Pa) above ambient pressure to avoid contamination with outside air. The chamber interior is filled with synthetic air (N$_2$, O$_2$, purity >99.9999%) and replenished through a flow controller as gas is lost to sampling extraction over the course of the experiment. The dilution rate for these experiments varied between 12–15 m^3 h^{-1}, which is 4–5.5% of the chamber volume per hour. Before each experiment, the chamber was purged with synthetic air at 200 m^3 h^{-1} overnight. A shutter system kept the chamber in darkness throughout experiments. The chamber setup includes standard instruments for measurement of temperature, pressure, humidity, and dilution flow. The ozone concentration was measured by chemiluminescence (modified ECO Physics CLD AL 700), and the β-pinene concentration was measured by Proton Transfer Reaction Mass Spectrometry (PTR-MS) (Lindinger et al., 1998), as relative to initial concentrations derived from injected β-pinene amount (Apel et al., 2009).

2.2 NO$_3$, N$_2$O$_5$, and NO$_{yi}$ measurements

The experiments were conducted as part of a large intercomparison campaign focused on measurements of NO$_3$ Dorn et al. (2009) and N$_2$O$_5$, Apodaca et al. (2009) during which ten different instruments for measurement of NO$_3$ and/or N$_2$O$_5$ were co-located at the SAPHIR chamber. Four instruments employed Cavity Ring-Down Spectroscopy (CRDS), three Cavity Enhanced Absorption Spectroscopy (CEAS), two Laser-Induced Fluorescence (LIF), one long-path absorption photometry (LOPAP), and one long-path Differential Optical Absorption Spectroscopy (DOAS). The NO$_3$ and N$_2$O$_5$ measurements across all instruments were found to

be in excellent agreement throughout the campaign, with instrumentation located within the chamber (DOAS and CEAS measurements) agreeing well with instruments sampling air from the chamber. Minor discrepancies among external sampling measurements were found to be due to filter losses of NO$_3$/N$_2$O$_5$. Filtering of aerosol was required for the high sensitivity (CRDS) measurements. In the figures we show NO$_3$+N$_2$O$_5$ from the NOAA Earth System Research Lab team (Dubé et al., 2006), but none of the conclusions of this manuscript depend strongly on the choice of the NO$_3$+N$_2$O$_5$ measurement, as the various measurements agreed well.

The Berkeley group measured NO$_2$ by LIF with excitation at 408 nm and total peroxynitrates (ΣPNs), total alkyl and multifunctional nitrates (ΣANs), and nitric acid (HNO$_3$) by subtraction of NO$_2$ signals from thermal dissociation to NO$_2$ in heated quartz ovens held at different temperatures ("NO$_2$-TD-LIF")(Thornton et al., 2000; Day et al., 2002). Details of this instrument, which varies from previous Berkeley designs in the laser wavelength and continuous-wave operation, are described in Farmer et al. (2009) and Fuchs et al. (2009). Fuchs et al. (2009) present a comparison of six NO$_2$ measurements in the SAPHIR chamber during the intercomparison, showing good agreement throughout the campaign across varying concentrations of H$_2$O and O$_3$.

The NO$_2$-TD-LIF instrument pulls sample air at 3 standard liters per minute (slpm) from ca. 10 cm above the floor of the SAPHIR chamber through a Teflon PFA inlet (40 cm of 3.2 mm inner diameter tubing), through a glass capillary orifice to reduce pressure, and splits it to four channels. The distance of 10 cm from the chamber wall was found to be sufficient to avoid sampling with a low bias due to wall loss induced concentration gradients. With the inlet oven at ambient temperature, NO$_2$ is detected. At the flow rates used in these experiments, ΣPNs, ΣANs, and HNO$_3$ dissociate to yield NO$_2$ at 180°C, 350°C, and 600°C, respectively. The mixing ratio of each class of nitrate is calculated from the difference in total NO$_2$ measured in adjacent temperature channels. In all ovens, we expect both gaseous and semivolatile aerosol-phase nitrates to dissociate completely. The instrument is blind to salts such as NaNO$_3$. The four oven channels are alternately sampled in two detection cells (P$\sim$1.5 Torr 200 Pa) pumped in series by a single laser. Comparison of the HNO$_3$ (gas + aerosol) channel of this instrument to a particle-into-liquid sampler (PILS) HNO$_3$ measurement in the presence of high NH$_3$ shows strong agreement (Fountoukis et al., 2007).

Laser-induced fluorescence is a highly sensitive technique for NO$_2$ detection. In the configuration employed here, a continuous-wave diode laser at 408 nm (8 mW, Toptica Photonics DL100) is used to excite NO$_2$ in the broad $A \leftarrow X$ electronic band. Red-shifted fluorescence ($\lambda > 650$ nm) is filtered and imaged onto a photomultiplier tube (PMT, Hamamatsu H7421-50) mounted at 90° to both the laser and sample flow on each cell. The two detection cells of this instrument had detection limits of 80/100 ppt 10 s^{-1} for NO$_2$ and 400/600 ppt 10 s^{-1} for ΣPNs, ΣANs, and HNO$_3$, accounting

for the 70–75 ppb NO$_2$ present in these experiments. Detection limits for this instrument were calculated as described by Day et al. (2002).

2.3 AMS and other particle instrumentation

An aerosol mass spectrometer (Aerodyne TOF-AMS) was operated to measure the aerosol chemical composition. The AMS was connected to the SAPHIR chamber via a stainless steel tube designed to minimize losses in the sampling line. The AMS working principles and modes of operation are explained in detail elsewhere (Canagaratna et al., 2007). In brief, an aerodynamic lens system at the instrument inlet is used to separate the gas phase from the aerosol particles. Aerosol particles are transferred through the vacuum system and impacted on a vaporizer which is typically held at $\sim$600°C to insure quick volatilization of the particles. Vapors are ionized with 70 eV electron impact ionization. A time of flight mass spectrometer is used for high resolution analysis of the chemical composition of these ions. As described in Sect. 3.5.1, the vaporizer temperature was varied between 150 and 600°C during parts of the experiments to derive additional information on the aerosol constituents.

For the extraction of chemically resolved mass concentrations of individual species the AMS raw data are typically evaluated with standard assumptions as described by Allan et al. (2004). In brief, this approach makes use of the reproducibility of mass spectral patterns of typical inorganic aerosol components such as ammonium, sulphate and nitrate. Subtracting from a measured mass spectrum the contributions of inorganic constituents and the contribution of gas phase sample, which is exclusively composed of N$_2$, O$_2$, H$_2$O and gases with mixing ratios in the ppm range, one obtains the mass spectrum of the organic aerosol. Due to the non-selective ionization with electron impact at 70 eV used in the AMS and the high fragmentation induced, further identification of individual molecules in a complex organic component is not possible. Nevertheless the high mass resolution mode of operation enables derivation of the overall elemental composition of the total organic content. Inorganic nitrate from e.g. NH$_4$NO$_3$ is detected as NO$^+$ (m/z 30) and NO$_2^+$ (m/z 46) with a typical ratio of NO$_2^+$:NO$^+$ of 0.35. In the W-mode (high mass resolution) of the TOF-AMS, possible interferences on mass to charge ratios 30 (e.g. CH$_2$O$^+$) and 46 (e.g. CH$_2$O$_2^+$) can be identified and accounted for in the further data evaluation. This option has been used for the experiments described here to derive the nitrate content and identity of the SOA. The quantification of the nitrate content of the SOA was performed based on calibrations with NH$_4$NO$_3$ aerosol. As described in Sect. 3.5.1, the ratio of NO$_2^+$:NO$^+$ was considerably lower than 0.35 throughout the experiments indicating that the aerosol did not contain significant amounts of inorganic nitrate or nitric acid.

Aerosol number concentrations and size distributions were measured with a Water Condensation Particle Counter (TSI
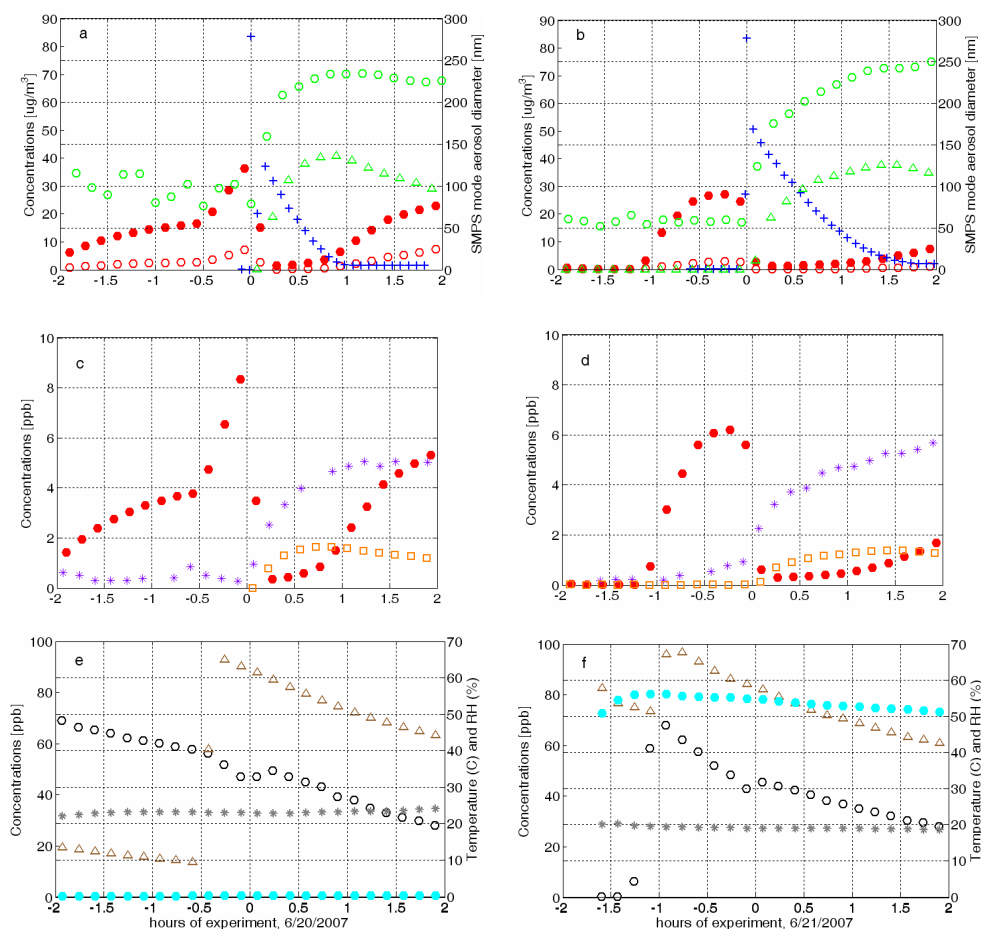
Fig. 1. Time evolution of N$_2$O$_5$+NO$_3$ (•), NO$_3$×10 (o) and β-pinene (+) mass concentrations and total particle mass loading (△) [μg/m^3] (not corrected for losses), as well as SMPS aerosol mode diameter (o) [nm], during the dry **(a)** and humid **(b)** experiments; time evolution of N$_2$O$_5$ +NO$_3$ (•), total alkyl nitrates (*) and aerosol nitrate (□) concentrations [ppb], during the dry **(c)** and humid **(d)** experiments; and time evolution of O$_3$ (△) and NO$_2$ (o) concentrations [ppb], temperature (*) [°C], and relative humidity (•) [%] during the dry **(e)** and humid **(f)** experiments.

WCPC model 3785) and a Scanning Mobility Particle Sizer (TSI SMPS model 3936, composed of a Differential Mobility Analyzer (DMA) model 3081 in connection with a WCPC 3785), respectively. The time resolution was 20 s for the CPC measurements and 7 min for the SMPS. SMPS size distributions were corrected for diffusion losses as described in the product manual (TSI, October, 2007). The total number concentration measured with the SMPS system and the CPC system agreed to within 10% with the CPC number concentration being larger than the SMPS concentration as expected from the different cut-off sizes. SMPS size distributions were converted into volume distributions for further comparison with the AMS mass distributions. The aerosol diameters measured with the SMPS (mobility diameter, d_m) and the AMS (vacuum aerodynamic diameter, d_{va}) are related via the following expression:

$$d_{va} = S \times \rho \times d_m \tag{1}$$

where S is a shape factor accounting for non spherical particles and ρ the particle density (DeCarlo et al., 2004). In the absence of additional information on particle shape (i.e., assuming S=1), the effective particle density can thus be derived from simultaneous measurements of the two diameters.

3 Results and discussion

### 3.1 Kinetics and mechanism of oxidation and SOA formation

The time series of gas and aerosol concentration measurements for the two NO$_3$+β-pinene experiments are shown in Fig. 1. To initiate each experiment, NO$_2$ and O$_3$ are added to the chamber that has been purged overnight with clean, dry air (12 complete air exchanges). NO$_3$ and N$_2$O$_5$ build up in the chamber, formed by the following reactions:
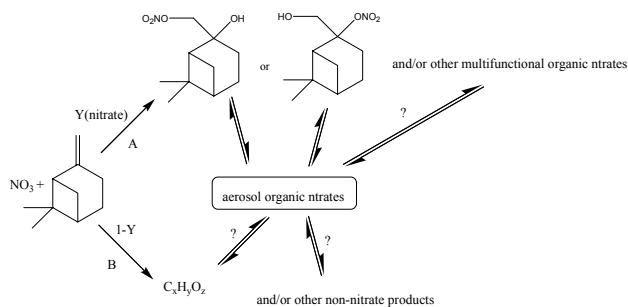
Fig. 2. NO$_3$+β-pinene reaction mechanism. Absorptive partitioning of the two explicit β-pinene hydroxynitrates is included in the model mechanism. The remaining pathways identified with ? are discussed in the text.

$$NO_2 + O_3 \rightarrow NO_3 + O_2 \qquad NO_3 + NO_2 \leftrightarrow N_2O_5 \qquad (R1)$$

At time -0.5 h in the dry experiment, the oxidant mixture is "charged" further by a second addition of 80 ppb O$_3$. At time 0 h in both experiments, β-pinene is added to the chamber and immediately begins reacting away via:

$$NO_3 + \beta - pinene \rightarrow hydroxynitrate \qquad (R2a)$$

$$NO_3 + \beta - pinene \rightarrow C_xH_yO_z \qquad (R2b)$$
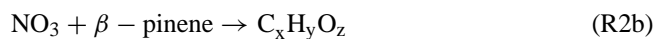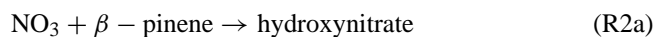
Because the NO$_3$+β-pinene reaction rate exceeds the decomposition rate of N$_2$O$_5$, the decomposition controls the initial rate of β-pinene consumption in these experiments. As NO$_3$ is depleted, N$_2$O$_5$ decomposes to yield NO$_3$+NO$_2$; hence, the measured N$_2$O$_5$+NO$_3$ is a proxy for total NO$_3$ available for reaction. Once the initially present reservoir of N$_2$O$_5$ has been consumed, the decay of β-pinene becomes rate limited by NO$_2$+O$_3$. Once the β-pinene is completely reacted, the NO$_3$+N$_2$O$_5$ concentration increases again. NO$_2$ and O$_3$ concentrations remain elevated (NO$_2$>10 ppb, O$_3$>40 ppb) throughout the experiments, providing a continuous source of oxidant (Fig. 1e and f).

Immediately upon initiation of the NO$_3$+β-pinene reaction, both gas- and aerosol-phase organic nitrates begin to build up in the chamber. The time traces of total gas- and aerosol-phase alkyl nitrates measured by TD-LIF and aerosol-phase nitrate measured by AMS are shown in Fig. 3. Concentrations are plotted as parts per billion (ppb) in these panels, as the molecular weight(s) of the nitrate(s) are unknown. Production of both gas- and aerosol-phase organic nitrates is prompt, with roughly the same amounts formed in both dry and humid experiments. In addition, the gas/aerosol partitioning appears similar in both experiments. This suggests that water vapor affects the gas-phase mechanism and partitioning into the aerosol phase minimally.

Quantitative nitrate formation branching ratios and gas/aerosol nitrate partitioning are determined by invoking a simple chemical mechanism (Fig. 2 and Table 2). We assume that the NO$_3$+β-pinene reaction forms either (A) a
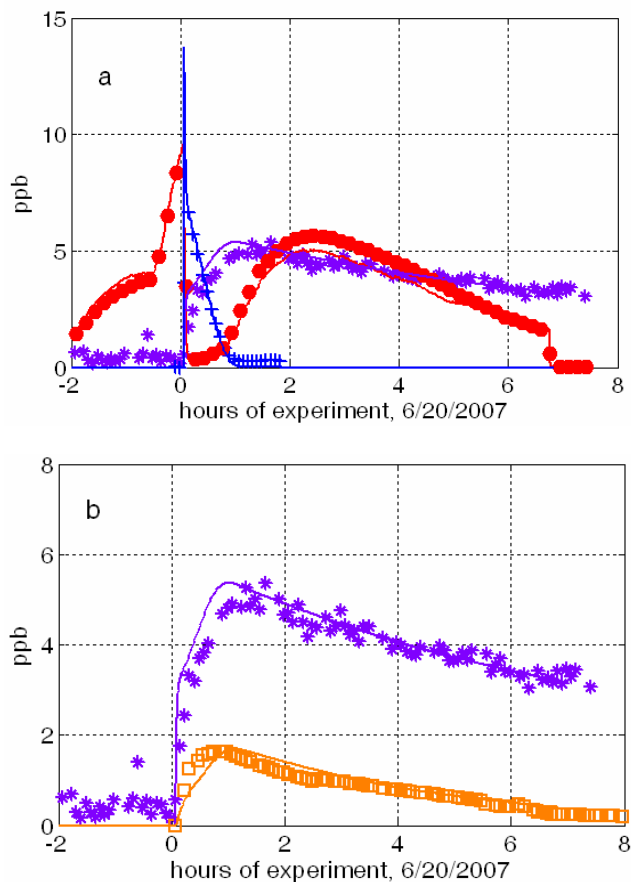
Fig. 3. Observations (symbols) and model calculations (lines) for dry NO$_3$+β-pinene experiment. **(a)** NO$_3$+N$_2$O$_5$ (•), β-pinene (+), and total alkyl nitrates (*). **(b)** Total (*) and aerosol phase (□) organic nitrate.

hydroxynitrate or (B) C$_x$H$_y$O$_z$. A chemical kinetics box model initialized with observed NO$_2$, O$_3$ and the mass of β-pinene injected, and constrained with the known rates of Reactions (R1–R3), observed dilution and wall loss and by the observed [NO$_3$] and temperature, is used to simulate the observations. The only variable parameter is the yield of organic nitrate (Y$_{nitrate}$=A/(A+B)) which is varied to reproduce the observed total alkyl nitrates signal (Fig. 1c and d).

The simple model invoked here is essentially an abbreviation of the Master Chemical Mechanism MCM v3.1 (Saunders et al., 2003), with explicit treatment of RO$_2$–RO$_2$ reactions replaced by a tunable branching ratio simply between hydroxynitrate and C$_x$H$_y$O$_z$ (non-nitrate organic) product channels. Ozone-initiated oxidation of β-pinene is less than 1% of NO$_3$ initiated oxidation except for the ~15 min immediately after initial N$_2$O$_5$+NO$_3$ depletion when the rate of O$_3$ with β-pinene approaches 10% of the NO$_3$ rate. Relative wall loss rates of NO$_3$ and N$_2$O$_5$ are determined from earlier no-hydrocarbon, no-aerosol experiments (k(NO$_3$-wall)=1.5×10^{-3} s^{-1} and k(N$_2$O$_5$-wall)

Table 2. Reactions and rate constant values in kinetics box model. Species shown in italics are not tracked in the model. OA is a counter species for organic aerosol. Quantities in bold are fit parameters in these experiments.

Reaction	Rate constant (cm^3 molecule^{-1} s^{-1} unless otherwise indicated)	Reference
NO$_3$ + BPIN → BPINNO3	**Y$_{nitrate}$** ×2.51×10^{-12}	(Calvert et al., 2000)
NO$_3$ + BPIN → CxHyOz	(1-**Y$_{nitrate}$**)×2.51×10^{-12}	(Calvert et al., 2000)
O$_3$ + BPIN → *products*	1.5×10^{-17}	(Calvert et al., 2000)
BPINNO3 + OA → BPINNO3AERO+2OA	k_{on}(**p$_{vap}$**)	see Sect. 3.4
BPINNO3AERO → BPINNO3 – OA	k_{off} s^{-1}	see Sect. 3.4
NO$_2$+O$_3$ → NO$_3$ + O$_2$	1.26×10^{-13} × exp(−2470/T)	0.9 × JPL Kinetics Data Evaluation #15 (Sander et al., 2006)
NO$_3$+NO$_2$ →N$_2$O$_5$	3-body rate; varies around ∼1.00×10^{-12} (298 K)	0.85×JPL #15 (Sander et al., 2006)
N$_2$O$_5$ →NO$_3$+NO$_2$	$k_{NO_3+NO_2}$/K_{eq}; K_{eq}=2.13×10^{-27}×exp(11025/T) s^{-1}	SAPHIR chamber observed K$_{eq}$
NO+O$_3$ →NO$_2$ + O$_2$	3.0×10^{-12} × exp(−1500/T)	JPL #15 (Sander et al., 2006)
O$_3$ → walls	3.68×10^{-6} s^{-1} (both)	Fit
NO$_3$ → walls	6×10^{-4} s^{-1} (dry) 3.3×10^{-3} s^{-1} (humid)	Fit
N$_2$O$_5$ → walls	7.2×10^{-5} s^{-1} (dry) 3.96×10^{-4} s^{-1} (humid)	Fit

=1.8×10^{-4} s^{-1}). These rates are scaled by a constant factor for each experiment, which in these two cases makes losses five times higher for the humid experiment than the dry. These wall losses are constrained by the NO$_3$/N$_2$O$_5$ concentration evolution prior to β-pinene injection. For numerical simplicity, aerosol wall loss for this kinetic modeling is determined by a fit to the decay in number density of aerosol for each experiment, which is found to be essentially equivalent to the wall loss determined by more sophisticated dynamical modeling used to calculate aerosol yields (see Sect. 2.2). These wall losses are significant for total nitrogen in the system, making it impossible to use nitrogen mass balance as a constraint on the analysis.

Y$_{nitrate}$ is found to be 40% (45%) in the dry (humid) NO$_3$+β-pinene experiments. The dry experiment is shown in Fig. 3, but the measurement/model agreement is comparable for the humid experiment. This model reproduces the alkyl nitrate signal throughout the 10-h experiment (Fig. 3a), with a maximum discrepancy of 15% during the first 5 min following injection of β-pinene, possibly resulting from the uneven mixing of the chamber on short timescales. The agreement of this model with the full observed alkyl nitrate time trace indicates that the first generation of oxidation chemistry is the only significant source of nitrates and that subsequent chemistry during the run does not convert the nitrates to non-nitrate species.

Humidity does not seem to affect the mechanism of organic nitrate formation appreciably, but a change in HNO$_3$ is observed. In the dry experiment, HNO$_3$ is produced continuously throughout the reaction, building up to 6 ppb at the end of the experiment. The continuous production throughout the dry experiment rules out a source from the initial concentrated radical mixture, such as

NO$_3$+RO$_2$→OH; OH+NO$_2$→HNO$_3$. The amount of HNO$_3$ produced greatly exceeds the expected HNO$_3$ production rate from NO$_3$+HCHO or another aldehyde. If we assume an aldehyde is produced one-to-one with C$_x$H$_y$O$_z$ in the non-nitrate channel (an upper limit), and it reacts with the aldehyde + NO$_3$ rate of 3×10^{-15} cm^3 molecule^{-1} s^{-1} (Atkinson, 1997), we only predict formation of 2 ppb of HNO$_3$ by 10 h. In the humid experiment, by contrast, the chamber HNO$_3$ concentration levels off at ∼2.5 ppb two hours after the β-pinene injection and remains steady. This difference in behavior is not understood, nor the formation mechanism for such a large amount of HNO$_3$. It is possible that reactive nitrogen is converted to HNO$_3$ on the chamber walls and that the desorption rate depends on RH. Another possible source of HNO$_3$ in the system is the heterogeneous reaction of NO$_3$ on organic aerosol surfaces, abstracting H from an alkane. Laboratory studies (Moise et al., 2002) have shown this process to have an uptake coefficient of order γ=0.0026 for alkanes. At the peak aerosol surface area measured during the dry experiment (5×10^{-6} cm^2 cm^{-3}), this translates to a lifetime of NO$_3$ uptake of ∼2.7 h.

An initial attempt was made to model the NO$_3$+β-pinene experiments using the full mechanism and branching ratios given in the Master Chemical Mechanism MCM v3.1 (http://mcm.leeds.ac.uk/MCM/), however, this model did not accurately reproduce our experimental results. While the observed organic nitrate yield is roughly reproduced using the full MCM, the details of the mechanism are not appropriate to describe our chamber experiments, which involved only a single monoterpene. In the MCM, the nitrato-alkylperoxy radicals generated by the initial NO$_3$ addition react with lumped RO$_2$ radicals, which are assumed to react analogously to CH$_3$O$_2$. These lumped RO$_2$

enable the formation of hydroxynitrates by β-hydrogen extraction, leaving the generic RO$_2$ partner as a carbonyl (RO$_2$+R(ONO$_2$)O$_2$→R(ONO$_2$)OH+R$_{-H}$O+O$_2$). In the case of our chamber experiments, the high-yield pathway is NO$_3$ attack on the terminal end of the double bond, yielding nitrato-alkylperoxy radicals *without β-hydrogens*.

An additional difference between the MCM model and our experiments is the predicted re-release of NO$_2$ and production of nopinone in the non-nitrate channel (our C$_x$H$_y$O$_z$ channel). The "burst" of additional NO$_2$ produced by this channel (NO$_3$+β-pinene→nopinone+HCHO+NO$_2$) in the MCM is not observed in our data. We have no direct measurement of the nopinone predicted to be produced in this channel. Nopinone yields from NO$_3$+β-pinene have not been well constrained by prior observations (Jay and Stieglitz, 1989; Barnes et al., 1990; Hallquist et al., 1999), and at least one study suggests that carbonyls other than nopinone are formed in significant yield: Hallquist et al. report a 12–14% yield of total carbonyls, but 0–2% yield of nopinone. In contrast, in O$_3$- or OH/NO$_x$-initiated SOA formation from β-pinene, the nopinone product has been observed by several groups (see Lee et al., 2006 and references therein) with yields of 15–40%.

The chemistry of the non-nitrate organic producing channel (C$_x$H$_y$O$_z$) is not understood. If the mechanism is adjusted to convert the NO$_2$ in the C$_x$H$_y$O$_z$ channel into a molecule that is invisible to all measurements, the predicted NO$_2$ time trace matches the observations. In addition, the model then better matches the measured O$_3$ decay (due to O$_3$+NO$_2$) during that time range. This observation is similar to results reported by Hoffmann et al. (1997), who found improved fit between measured and modeled NO$_2$ concentrations in the NO$_3$+β-pinene system if the reaction converting a nitratoalkyoxy radical to a carbonyl and releasing NO$_2$ was deleted from their mechanism. In that case, the authors suggested the formation of dinitrates. In our case, the nitrogen in the non-nitrate organic forming channel of this reaction appears to be converted chemically to a species that either immediately partitions to the walls, or to which our NO$_y$ instrument is not sensitive, because dinitrates would appear simply as a doubled yield of organic nitrate. This "invisible" reactive nitrogen may be the slow source of HNO$_3$ over longer timescales. While the gas-phase mechanism remains unclear, the inability to measure nitrogen mass conservation has no impact on our later conclusions about gas/aerosol partitioning of organic nitrates or aerosol yield.

Based on the β-pinene structure, the nitrato-peroxy radicals formed in the initial step of NO$_3$ oxidation in these experiments have the possibility to undergo an additional radical propagation isomerization to yield more highly substituted oxidized species. A recent paper (Gong et al., 2005) shows that a straight-chain alkoxy radical with a δ-hydrogen can undergo isomerization to form a δ-hydroxy-peroxy radical, which reacts with another RO$_2$ to form a diol or hydroxycarbonyl. The structure of the β-pinene
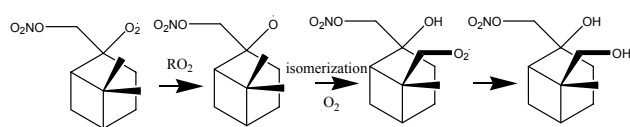
Fig. 4. Proposed isomerization mechanism for the initial nitrato-alkoxy radical leading to β-pinene dihydroxynitrates.

derived nitrato-peroxy radical contains a δ-hydrogen situated for isomerization. By analogy, the isomerization chain shown in Fig. 4 could lead to multiply-substituted organic nitrates of β-pinene, such as the β-pinene dihydroxynitrate (MW=231 g mole^{-1}) shown.

3.2 Aerosol yield

The aerosol production in our experiments occurs in two stages. Very soon after the initiation of the NO$_3$+β-pinene reaction, aerosol particles are produced by nucleation. After this initial burst, the particulate mass growth is caused by the growth of the existing particles, not by generation of new nuclei. During the growth period, aerosol particles are lost to deposition to the chamber walls as well as being flushed out due to the sampling flow. These losses also cause a loss of aerosol mass. Particle number is also lost by coagulation of particles; this process, however, conserves the total aerosol mass.

The dilution losses of the aerosol were calculated from the measured chamber flows and the aerosol size distribution data measured by the SMPS. Dilution was assumed to be independent of particle size. The wall loss rate was estimated to be mainly due to diffusion; the loss rate constant was estimated to be proportional to the square root of the particle diffusion coefficient (Verheggen and Mozurkewich, 2006). The loss rate constant, β, is given by:

$$\beta(r) = C_{\text{fit}}\sqrt{D_P(r)} \tag{2}$$

where C_{fit} is an empirical fitting coefficient and $D_P(r)$ is the radius-dependent particle Brownian diffusion coefficient. C_{fit} was numerically fitted using a sectional aerosol dynamical model (Korhonen et al., 2004) together with a control experiment with ammonium sulphate aerosol where no condensation was occurring; the value obtained was C_{fit}=0.25.

Particle volume dilution and wall losses were calculated by computing the size-dependent particle number losses for each measured SMPS spectrum. For these experiments, the wall losses caused between 10–20% of the particle volume loss; the rest of the loss was caused by dilution.

The time evolution of total particle mass loading during the dry and humid experiments shown in Fig. 1a and b are lower limits of the amount of aerosol produced in each experiment, because these raw data do not include a correction for loss of aerosol to the chamber walls or dilution. In order to determine a quantitative aerosol yield for each experiment,

Table 3. Reagent concentrations and SOA yields determined immediately after consumption of β-pinene is complete.

Temperature/ RH	β-pinene(peak) ($\mu g\,m^{-3}$)	N_2O_5(peak) ($\mu g\,m^{-3}$)	ΔM_{corr}(peak) ($\mu g\,m^{-3}$)	SOA Yield
293–301 K/<0.5%	90	35	48	53%
291–293 K /42–56%	90	28	41	46%
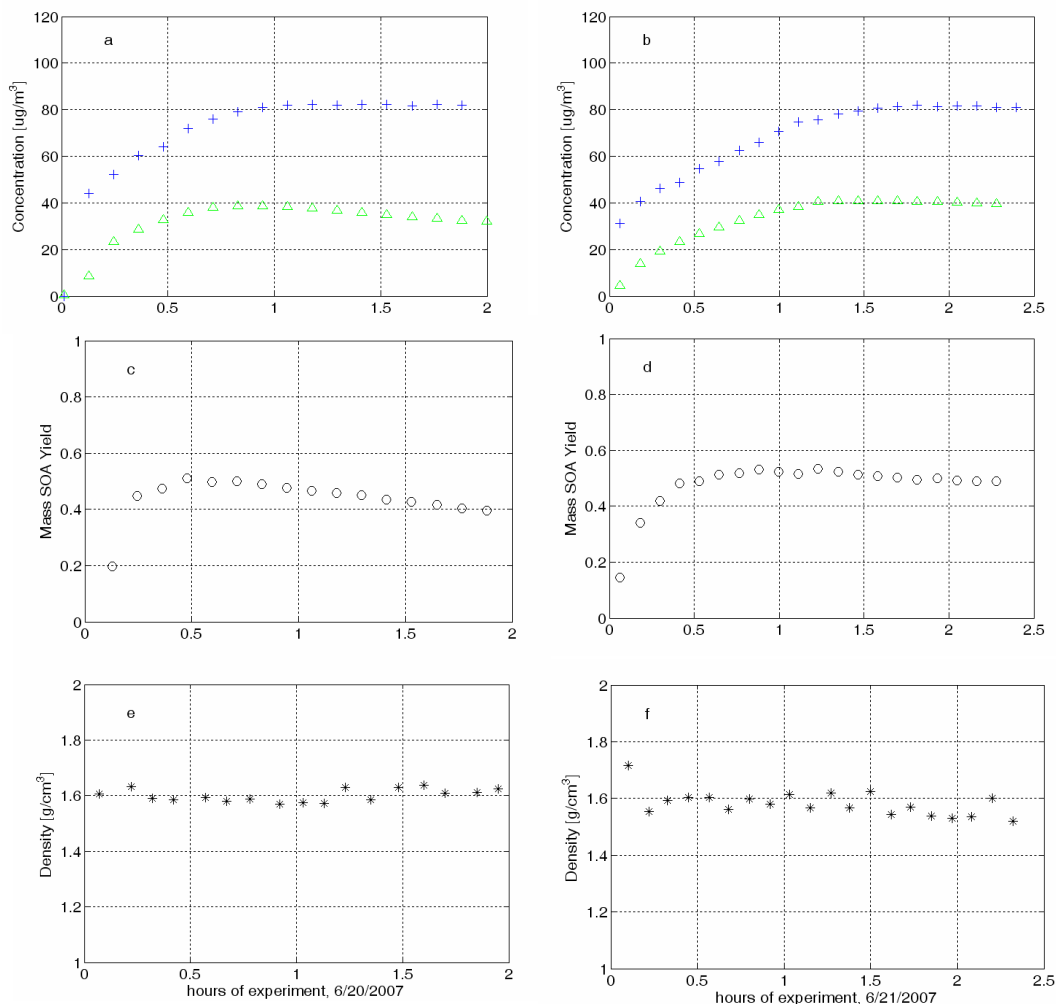
Fig. 5. Time evolution of β-pinene reacted (+) and mass aerosol formed (Δ) (using measured density) during the dry **(a)** and humid **(b)** experiments; mass yield (o) for dry **(c)** and humid **(d)** experiments; and density (*) determined from comparison of AMS and SMPS measured mode diameter, for the dry **(e)** and humid **(f)** experiments. Peak mass yield (calculated immediately after all β-pinene is consumed) is $\sim$50% under both dry and humid conditions.

we correct the aerosol mass loading for these losses using the loss rate determined by the aerosol dynamical model described above. We then calculate the yield as:

$$Y = \frac{\Delta M}{\Delta VOC} \qquad (3)$$

where ΔM is the corrected aerosol mass loading ($\mu g\,m^{-3}$)

and ΔVOC is the total reacted concentration ($\mu g\,m^{-3}$) of β-pinene. The wall loss + dilution corrections are approximately 1% at 30 min, 15% at 3 h, and 25% at 8 h for the dry experiment, and 3% at 30 min and 11% at 3 h for the humid experiment (no volume data were available at later times). The final SOA yields (Table 3) measured at the conclusion of each experiment were $\sim$50% for both experiments.

The corrected aerosol mass yield (Fig. 5) increases as the β-pinene is consumed, then gradually decreases after the β-pinene is entirely consumed. This is in contrast to the typical Odum/Pankow interpretation of SOA yield, in which yield increases with increasing mass of organic aerosol (M_o) (Pankow, 1994a, b; Odum et al., 1996). The fact that SOA yield does not monotonically increase with increasing organic aerosol mass suggests that volatilization of the aerosol competes kinetically with condensation of SOA. Although the organic nitrates seem to be in gas/particle equilibrium (see Sect. 3.4), the remaining constituents of the aerosol appear to undergo further reactions to yield more volatile products that return to the gas phase.

Evidence for particle evaporation in the dry experiment can also be seen in the observed aerosol size distribution. Using size distribution and total volume time traces, one can approximate the particle growth rate at each time step. During the NO$_3$+β-pinene reaction, the (positive) growth rate is proportional to the amount of β-pinene in the chamber. After all the β-pinene is consumed, the growth rate becomes negative, with a constant evaporation rate of 5 nm hr^{-1} for the remainder of the (dry) experiment. This suggests further chemical evolution in the aerosol phase yielding more volatile products. Another possibility is that the evaporation of the particles results from re-equilibration in response to more rapid wall uptake of the gas-phase alkyl nitrates in the dry chamber.

By contrast, the humid experiments showed less decrease in SOA yield over time. The solvating presence of adsorbed water may inhibit particle revolatilization, or the existence of water vapor may alter the gas phase reaction mechanism of the organics to avoid producing species that could further react in the aerosol particles. The average temperature during the humid experiments was approximately 2°C lower than the dry experiment (Fig. 1e and f). It is possible that this temperature difference was sufficient to inhibit revolatilization of the particles in the cooler humid experiment.

3.3 Role of organic nitrates in nucleation and particle growth

As can be seen in Fig. 6, organic nitrates appear to play a role in both nucleation and particle growth processes. Figure 6a shows the first hour of the experiment, demonstrating that organic nitrates are observed as soon as any aerosol is detected (the AMS measures particles above 30 nm in diameter, preventing direct measurement of the nucleating species). In Fig. 6b, however, it is clear that at long times there is a constant concentration of gas-phase organic nitrate. These observations seem contradictory: if organic nitrate aerosol formation is an equilibrium process with a certain vapor pressure of organic nitrates existing over the aerosol, that amount of gas phase nitrate should be required to build up before homogeneous nucleation begins. The observation of nitrates in the first particles, however, suggests that a different nitrate
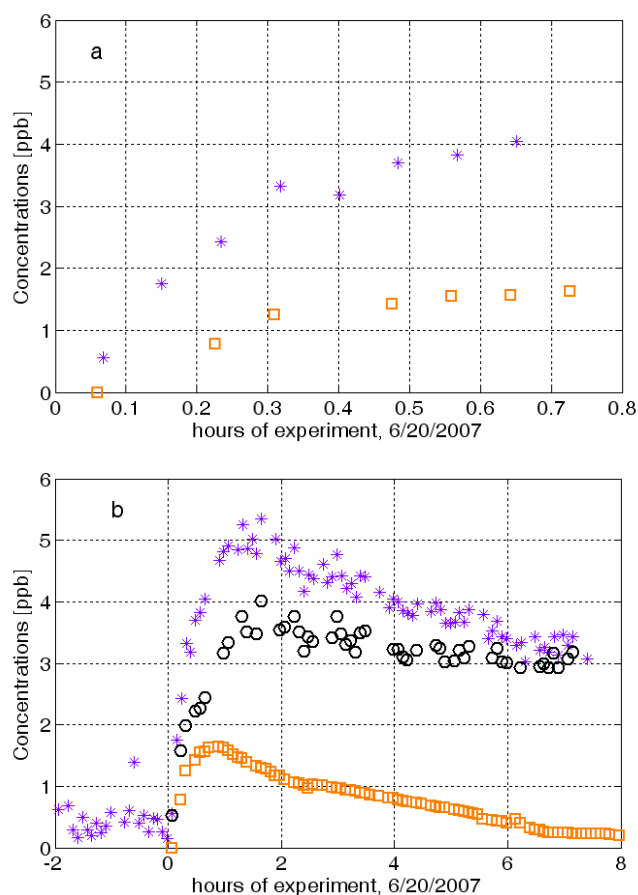
Fig. 6. (a) First 0.8 h of the time evolution of total alkyl nitrates (*) and aerosol organic nitrate (□) concentrations [ppb] during the dry experiment. **(b)** Time evolution of total alkyl nitrates (*), aerosol organic nitrate (□), and gas-phase organic nitrate (o) determined subtractively.

species with much lower vapor pressure also plays a role in the nucleation process.

This apparent contradiction might be explained by the existence of distinct nucleating and condensing species. Burkholder et al. (2007) successfully reproduce nucleation and particle growth observed after the O$_3$- and OH- initiated oxidation of α-pinene and β-pinene using a model with tunable yields of nucleating and condensing species. In all cases, the nucleating species was found to have a significantly lower yield (Φ_{Nuc}=0.00005–0.009) than the condensing species (Φ_{Con}=0.06). One suggestion of what these condensing species might be comes from chamber studies of NO$_3$+isoprene (Ng et al., 2008), where chemical ionization mass spectrometry (CIMS) indicated the presence of nitrated organic peroxide isoprene dimers. In the case of β-pinene, these C$_{20}$ organic peroxides would have the very low volatility required to affect nucleation. In our experiments, a low-yield nitrate product such as this peroxide may be responsible for nucleation, while the longer-term particle growth is

driven by the 40–45% organic nitrate channel. Our kinetic modeling did not explicitly treat the nucleation process; we simply introduced the abrupt increase in aerosol number concentration as it was observed, then allowed gas-aerosol partitioning to proceed.

3.4 Gas/aerosol partitioning and determination of p_{vap} of condensing nitrate

Gas/aerosol partitioning of the organic nitrate is parameterized following the absorptive partitioning formalism (Pankow, 1994a, b; Capouet et al., 2008):

$$K_p = \frac{F/\text{TSP}}{A} = \frac{760 \cdot RT \cdot f_{om}}{\text{MW}_{om} \cdot 10^6 \cdot \zeta \cdot p_{vap}} \tag{4}$$

This framework of partitioning is described as "absorptive" because it implies that the fractionation between gas and aerosol phase of semivolatile species is dependent on the amount of aerosol phase already available. In the above partitioning coefficient expression, F and A are the total aerosol-phase and gaseous concentrations of the compound of interest, and TSP is the concentration of total suspended particulate matter. In the second expression in terms of thermodynamic properties, R is the universal gas constant (8.206×10^{-5} atm m^3 K^{-1} mol^{-1}), T is temperature (K), f_{om} is the weight fraction of organic matter in the total aerosol (=1 for these experiments), MW_{om} is the average molecular weight of the absorbing organic material (g mole^{-1}), ζ is the activity coefficient of the compound of interest in the organic phase (assumed=1 for these experiments), and p_{vap} is the vapor pressure of the compound of interest (Torr); 760 (Torr atm^{-1}) and 10^6 (μg g^{-1}) are conversion factors. This gives K_p in units of m^3 μg^{-1}.

In order to implement this partitioning in our model, we employ a kinetic representation of this partitioning expression (Kamens et al., 1999):

$$K_p = \frac{k_{on} \cdot N_{Avo}}{\text{MW}_{om} \cdot 10^{12} \cdot k_{off}} \tag{5}$$

where k_{on} and k_{off} are the absorption (cm^3 s^{-1} molecule^{-1}) and desorption (s^{-1}) rates of the compound of interest to the aerosol, N_{Avo} is Avogadro's number (6.023×10^{23} molecule mole^{-1}), MW_{om} is as defined above, and 10^{12} (μg g^{-1} cm^3 m^{-3}) is a conversion factor.

Finally, we use an expression for the absorption rate of a gas by a particle (k_{on}) (Lelieveld and Crutzen, 1991):

$$k_{on} = \frac{\text{MW}_{om}}{\rho N_{Avo}} \cdot \left(\frac{a^2}{3D_g} + \frac{4a}{3\omega\gamma} \right)^{-1} \tag{6}$$

where MW_{om} and N_{Avo} are as defined above, ρ is the aerosol density (measured by comparison of AMS and SMPS mode diameters to be 1.6 g cm^{-3} throughout both the dry and humid experiments), a is the average aerosol radius (cm), taken at each time step from measured aerosol volume density and

number density, D_g is the diffusivity in the gas phase of the assumed MW=215 g mole^{-1} condensing species as calculated by the Fuller method (Poling et al., 2001), ω is the mean gas phase molecular speed of this species (cm s^{-1}), and γ is the dimensionless accommodation coefficient of the organic species onto organic aerosol. In the absence of accommodation coefficient data for this system, we assume γ=0.2, which was used by Capouet et al. (2008) in simulating α-pinene photo-oxidation.

In order to implement Eqs. (4–6) in our modeling, we add absorption of the organic nitrate product onto aerosol (k_{on}; BPINNO3$_g$ + OA$\rightarrow$BPINNO3aero) and desorption off aerosol (k_{off}; BPINNO3aero$\rightarrow$BPINNO3$_g$) as chemical reactions in the kinetics model, keeping track of organic aerosol mass as the nitrate adsorbs and desorbs. Constraining the model to reproduce the observed time traces of total and aerosol organic nitrate (Fig. 3b) using the vapor pressure of the condensing nitrate (p_{vap}) as the fitting parameter gives p_{vap}=4×10^{-6} Torr=5.33×10^{-4} Pa (5×10^{-6} Torr=6.67×10^{-4} Pa) in the dry (humid) $NO_3 + \beta$-pinene experiments.

3.4.1 Group contribution method estimated p_{vap}

To provide a comparison for the vapor pressure consistent with the kinetics modeling, we employ a group contribution method (Capouet and Müller, 2006). This calculation of vapor pressure assumes that functional groups have an additive effect on the vapor pressure of a molecule, which can be described as:

$$\log_{10} p_{vap}(T) = \log_{10} p_{vap,hc}(T) + \sum_{k}^{n} \nu_k \tau_k(T) \tag{7}$$

where $p_{vap,hc}$ is the vapor pressure of the alkane "parent" compound, which has the same carbon backbone but only hydrogen functionalities, ν_k is the number of functionalities of type k in the compounds, n is the number of types of oxygenated functionalities, and τ_k are the group contribution parameters for each functionality type k (which also depend on the degree of substitution of the carbon bearing the functionality). The parent compound vapor pressure and group contribution parameters are all temperature dependent; in this case we estimate all parameters at 298 K.

We assume the condensing species in these experiments are hydroxynitrates, as shown in Fig. 2. We calculate the vapor pressures of the two structural isomers of β-pinene hydroxynitrate. The parent compound for these species is the same alkane as for α-pinene, as these two hydrocarbons differ only in the location of the double bond. The value for $\log_{10} p_{vap,hc}(298)$, taken from Capouet and Müller (2006) is 0.4232. The relevant group contribution values for the dominant isomer, in which the NO$_3$ radical attack occurs at the terminal end of the double bond, leading to a structure with primary nitrate and tertiary hydroxyl functionality, are τ_{ONO2p}=-2.0897 and τ_{OHt}=-1.4418. The relevant

values for a primary hydroxyl and tertiary nitrate functionality for the second isomer are, respectively, $\tau_{OHp}=-2.6738$ and $\tau_{ONO_2t}=-1.2793$. These values give the following vapor pressures for the two β-pinene hydroxynitrates ("tert" reconsumption in these "prim" referring to the primary terminal nitrate):

$$\log_{10} p_{vap,prim}(298) = 0.4323 - 2.0897 - 1.4418 = -3.1083$$
$$\rightarrow \quad p_{vap,prim} = 10^{-3.1083} = 7.79 \times 10^{-4} \text{ Torr} = 1.04 \times 10^{-1} \text{ Pa}$$

$$\log_{10} p_{vap,tert}(298) = 0.4323 - 2.6738 - 1.2793 = -3.5299$$
$$\rightarrow \quad p_{vap,tert} = 10^{-3.5299} = 2.95 \times 10^{-4} \text{ Torr} = 3.93 \times 10^{-2} \text{ Pa}$$

A weighted average of these vapor pressures, using the 80:20 ratio reported in the MCM for primary:tertiary nitrate gives an average vapor pressure of 3.41×10^{-4} Torr (4.55×10^{-2} Pa), two orders of magnitude higher than the value inferred from the observations.

This vapor pressure indicates a significantly more volatile species than the model fit p_{vap} of 4–5×10^{-6} Torr (5–7×10^{-4} Pa) suggests. However, the addition of one further primary hydroxyl group, such as by the mechanism shown in Fig. 4, leads to a lowering of vapor pressure. The value for this additional functional group is $\tau_{OHp}=-2.6738$, leading to $p_{vap,tri-functional}=1 \times 10^{-6}$ Torr (1.33×10^{-4} Pa), in near agreement with the partitioning model. We propose that this dihydroxy nitrate structure, with molecular formula $C_{10}H_{17}O_5N$ (MW=231 g mole^{-1}), or a similar multifunctional molecule with three oxidized functional groups, is responsible for the high aerosol yield from this reaction.

## 3.5 Aerosol chemical composition

3.5.1 Organic nitrates

In addition to the TD-LIF evidence for nitrate yields of 40–45%, our measurements indicate that the nitrate (NO₃⁻) signal observed in the AMS is due only to organic nitrates, and not the condensation of HNO₃ (inorganic nitrate). Nitric acid has a vapor pressure of 7 Torr (930 Pa), several orders of magnitude higher than that predicted for the condensing species, but is removed rapidly by surfaces (Dubowski et al., 2004) and is highly soluble in polar matrices such as water. Two lines of reasoning derived from distinct measurements rule out HNO₃ as a contributor to the aerosol phase. First, Fig. 7 shows time traces of AMS aerosol nitrate (NO₃⁻) versus total alkyl nitrates and HNO₃ as measured by TD-LIF. The aerosol nitrate time trace is correlated with alkyl nitrates and not with nitric acid, indicating that it is not formed by simple condensation of HNO₃ onto aerosol. Second, a similar conclusion is drawn from the AMS data. The NO₂⁺:NO⁺ ratio (m/z 46:m/z 30) measured during NO₃+β-pinene experiments was ~1:10, regardless of impactor heater temperature (150–580°C). In contrast, the NO₂⁺:NO⁺ ratio measured by the same AMS sampling laboratory-generated ammonium
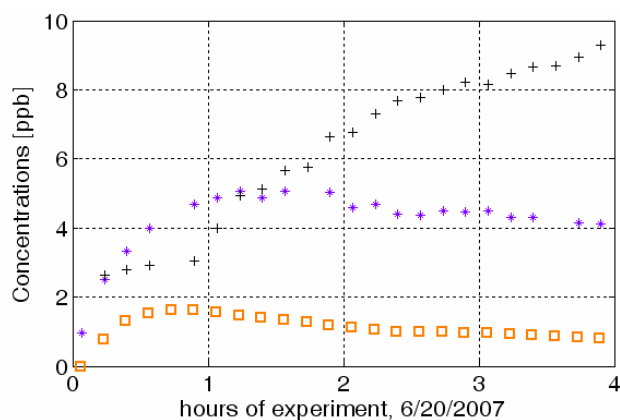
Fig. 7. Time evolution of total alkyl nitrates (*), HNO₃ (+), and aerosol organic nitrate (□) concentrations [ppb] during the dry experiment.

nitrate (NH₄NO₃) aerosol was ~1:2.7. This latter number is broadly consistent with reported ratios for ammonium nitrate measured by other AMS groups, which have ranged from m/z 46:m/z 30 of 1:2 to 1:3 (Alfarra et al., 2006) to m/z 46:m/z 30 of 1:1.18 (Cottrell et al., 2008). The ratio observed for the NO₃+β-pinene produced SOA is clearly distinct from these inorganic nitrate fragmentation patterns.

During one portion of each NO₃+β-pinene experiment, the AMS inlet vaporizer temperature was lowered temporarily. In the dry experiment the vaporizer temperature was decreased in ten steps from 570°C to 145°C, measuring for 15 to 30 min on each temperature. For the humid experiment the vaporizer was held at 570°C (majority of experiment), 395°C (28 min), and 148°C (30 min). As temperature was lowered, total organic aerosol mass measured decreased, while total nitrate aerosol mass remained constant. This is interpreted to mean that the total signal obtained at the minimum vaporizer temperature of 145°C (dry experiment) originates from organic nitrate, allowing an estimation of its molecular weight. The following assumptions are made. The organic nitrate is measured as NO⁺ and NO₂⁺ and a broad variety of other ions which are summed under the organic component. The mass ratio of the total organic to the sum of NO⁺ and NO₂⁺ is assumed to be equal to the molecular weight ratio of the pure organic part and the nitrate part of the organic nitrate. This relies on the assumption that only the organic nitrate is present at this lowest temperature. Thus, the minimum measured organic to nitrate ratio of 2.7±0.2 in the dry experiment is used to estimate the molecular weight of the organic nitrate present. This yields a molecular weight of 229±12 g mole^{-1} for the organic nitrate, well in the range of the proposed structures (215 or 231 g mole^{-1}; see Fig. 4). The minimum ratio organic/nitrate observed in the humid experiment was 6±0.4 at a vaporizer temperature of 148°C. Assuming again that the total signal obtained
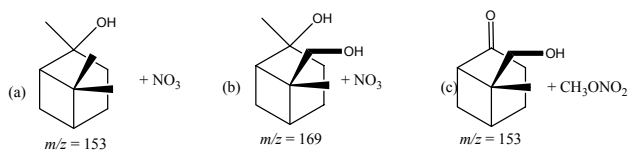
Fig. 8. Potential identification of m/z=153 and 169 fragments, which are correlated with aerosol nitrate.

is exclusively from organic nitrates we obtain a molecular weight of 434±25 g mole^{-1}. This greatly exceeds the molecular weight of the structures proposed and indicates that either the identity of the organic nitrates is considerably different in the humid case or a larger fraction of more volatile pure organic components contributes to the signal obtained at the lowest vaporizer temperatures when the humidity is high.

An additional piece of information about aerosol composition can be gained by looking at the ratio of organic to nitrate mass measured by the AMS with the vaporizer at ~600°C over the course of the experiments. In both the dry and humid cases, this ratio throughout the experiment is ~8–10, indicating a reasonably consistent aerosol composition. If we assume that the organic nitrate present is a 215–231 g mole^{-1} hydroxynitrate or dihydroxynitrate (C$_{10}$H$_{17}$O$_4$N or C$_{10}$H$_{17}$O$_5$N), this means that a roughly constant 32–41% of total aerosol mass is organic nitrate. The fraction of aerosol that is organic nitrate can also be calculated by comparing the AMS and SMPS aerosol mass measured during the periods of low (145–148°C) vaporizer temperature, when it is assumed that the AMS measured only organic nitrate. The ratio of AMS : SMPS mass under these conditions is 4.5±0.3 μg m^{-3} : 11.6±0.6 μg m^{-3}, which gives an organic nitrate contribution to total SOA mass of 4.5/11.6=39%, similar to the above estimates.

Insight into the structure of this aerosol organic nitrate can be derived from the AMS spectra. Throughout the experiments, a bimodal peak at m/z 153 is observed which is correlated with the aerosol nitrate signal (R^2=0.79 for the dry experiment, R^2=0.88 for the humid). The high resolution W-mode operation of this AMS instrument allows assignment of the two major component fragments at this mass as C$_{10}$H$_{17}$O$^+$ and C$_9$H$_{13}$O$_2^+$. A smaller peak at m/z 169 is also correlated with aerosol nitrate signal, which can be assigned as C$_{10}$H$_{17}$O$_2^+$. These fragments can speculatively be identified (Fig. 8) as organic fragments from the mono- and dihydroxynitrates of β-pinene, with C$_{10}$H$_{17}$O$^+$ corresponding to loss of NO$_3$ from the monohydroxynitrate (A), C$_{10}$H$_{17}$O$_2^+$ corresponding to loss of NO$_3$ from the dihydroxynitrate (B), and C$_9$H$_{13}$O$_2^+$ corresponding to loss of CH$_3$ONO$_2$ from the dihydroxynitrate, leaving a hydroxyketone (C).
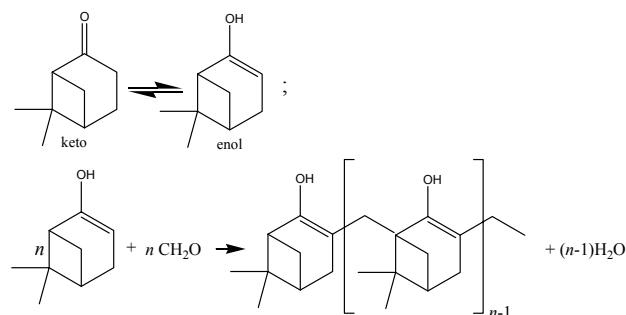
Fig. 9. Keto-enol equilibrium for nopinone; potential polymerization mechanism via enol form of nopinone.

3.5.2 Non-nitrate organic compounds

The most reasonable structure for the non-nitrate C$_x$H$_y$O$_z$ channel product in the NO$_3$+β-pinene reaction is nopinone, based on RO$_2$-RO$_2$ self-reaction and loss of NO$_2$. Nopinone is included in the MCM mechanism as the non-nitrate product of this reaction. By the group contribution method employed here to estimate organic nitrate volatilities, nopinone would have a vapor pressure of p_{vap}=4.8×10^{-2} Torr=6.4 Pa ($\tau_{carbonyl}$=−0.8937, Capouet and Müller, 2006), indicating a volatile species unlikely to condense appreciably into the aerosol phase. However, the above calculations indicate that a significant amount of organic mass must co-condense with the organic nitrates.

Another intriguing piece of information comes from the NO$_3$+β-pinene study of Hallquist et al: although the authors had a specific FTIR fingerprint for nopinone, in all experiments they observed no or maximum 1–2% nopinone formed. They did observe carbonyl groups to be formed at about 12–14% molar yield, compared to the 60–70% yield of nitrate. By contrast, in the NO$_3$+α-pinene experiments, they observed ~70% yield of carbonyls, with essentially all of that carbonyl signal accounted for by the known pinonaldehyde product. This suggests that the chemistry of the C$_x$H$_y$O$_z$ channel is unknown.

Nopinone is a ketone with no α-hydrogens, so it is not likely to be reactive with NO$_3$. However, a possible mechanism for further reaction of the nopinone product is the keto-enol isomerization, forming a double bond in the β-pinene ring that may be reactive to further oxidation and formation of multifunctional organics or oligomers. This oligomer formation may be facilitated by the co-presence of formaldehyde in a mechanism analogous to the well-known phenol-formaldehyde step-growth polymer formation reaction, (Cowie, 1991). The keto-enol equilibrium and potential oligomerization reactions are shown in Fig. 9. These higher-molecular weight compounds would in turn be more likely to partition to the aerosol phase. At least one reactor study with FTIR analysis of the products of O$_3$+β-pinene (Winterhalter et al., 2000) did not find evidence of keto-enol

tautomerism leading to polymer formation – sustained high concentrations of nopinone and HCHO were observed in that study. Nevertheless, for some reason high nopinone yields have not been observed from NO$_3$+β-pinene, and the experiments presented here suggest that there must exist some mechanism by which the organic compounds in that reaction channel become less volatile.

3.6 Comparison to previous results

To our knowledge, only one previous study has measured the aerosol mass yield from NO$_3$+β-pinene. Hallquist et al. (1999) conducted experiments in the EUPHORE facility in Valencia, Spain investigating product yields and aerosol formation from NO$_3$ oxidation of several monoterpenes including β-pinene, employing long-path FTIR to study the products. At the lowest initial [N$_2$O$_5$] of 7 ppb and [β-pinene] of 18 ppb, the conditions most comparable to our experiments, they observed a molar nitrate yield of 61% using FTIR (compared to our 40–45%) and mass aerosol yield using SMPS of 10% (compared to our ∼50%). While the nitrate differences are relatively small, the aerosol yield difference is significant and its source is not clear at this time.

Several additional studies of aerosol formation from NO$_3$-initiated oxidation of β-pinene, though they do not report yields, are relevant. Bonn and Moortgat (2002) reacted 50 ppb α- or β-pinene with 1 ppm NO$_3$+N$_2$O$_5$ oxidant (fully two orders of magnitude higher concentration than the ∼10 ppb used here). They observed *no* new particle nucleation. They also reported observing "memory effects" in a steady-state flow tube experiment on the same chemical system. Throughout their NO$_3$ experiments, particle concentrations rose continuously as conditions were changed, not returning to same initial values as they did in O$_3$ experiments. They interpret this as the result of some NO$_3$ reservoir species depositing to the walls and then returning to the gas phase over time, to generate more particles.

The Jülich SAPHIR chamber is operated to avoid wall permeation and such effects, by overnight purging before experiments and the maintenance of a nitrogen-purged volume between the double walls of the chamber. This should prevent any day-to-day "memory effects" of the chamber walls. However, on the timescale of an individual experiment, it may be that the same nitrogen-containing species as in the Bonn and Moortgat experiments are depositing to the walls, to be released by subsequent chemistry on the surfaces. A point of agreement between our results and those of Bonn and Moortgat is in the observation of no water effect (from RH<0.01% to 25% in their experiments and from RH<0.5 to 56% in our experiments) on particle size distribution. In addition, they were able to rule out HNO$_3$ condensation as the source for nucleation in the NO$_3$+β-pinene system, in agreement with our observation that aerosol nitrate is organic in nature, and not HNO$_3$.

In comparing chamber SOA yields and attempting extrapolation to the real atmosphere, it is important to recognize that the radical chemistry in chambers may vary and may not be representative of ambient conditions. SOA yields have been shown to be sensitive to HO$_2$/RO$_2$ concentration ratios (Docherty and Ziemann, 2003). In chamber experiments, HO$_2$/RO$_2$ can be of order 2×10^{-3}–4×10^{-2} (Jenkin, 2004), with variation due to the use or lack of OH scavengers. In the case of β-pinene chamber studies this ratio is likely to be particularly perturbed, because most of the RO$_2$ formed are tertiary peroxy radicals with no possibility of HO$_2$ formation. Modeling of our chamber conditions suggests very low HO$_2$/RO$_2$ ($<10^{-4}$ during the reactive period of the experiment), with the result that less than 1% of RO$_2$ radicals react with HO$_2$. In contrast, field measurements found ambient HO$_2$/RO$_2$ ratios close to 1 (Hanke et al., 2001). This suggests that in the real atmosphere, more nitrooxy hydroperoxides may be formed than in our chamber experiments, as noted in a comprehensive review of tropospheric VOC chemistry (Atkinson, 1997). It is unclear how this difference would affect the atmospheric NO$_3$+β-pinene SOA yield. Therefore, in the following section, we use the chamber measured yield but encourage consideration of this limitation of the measurement.

3.7 Estimated atmospheric source of SOA from NO$_3$+β-pinene

To assess the contribution of NO$_3$+β-pinene products to atmospheric SOA loading, we use the measured 50% mass yield in conjunction with estimates of the fraction of β-pinene emissions which are consumed by NO$_3$. Because this fraction will have large regional and temporal variability corresponding to the overlap of regions of high NO$_x$ and O$_3$ with monoterpene emissions, an accurate estimate of the SOA source requires use of a spatially resolved regional or global model. We make two independent source estimates, one deriving from a regional model and one based on a previous global estimate.

In California, July average monoterpene emissions are estimated to be ∼ 60 tons hr^{-1}, using a statewide version of the Biogenic Emission Inventory Geographic Information System (BEIGIS), currently in development (personal communication, Klaus Scott, CARB; a previous version of BEIGIS is described by Scott and Benjamin, 2003). Of these monoterpene emissions, ∼30% occur at night (Sakulyanontvittaya et al., 2008), and ∼25% are β-pinene (Griffin et al., 1999a); (Guenther et al., 1995). This gives a regional estimate of the California nighttime β-pinene source of 4.5 tons hr^{-1}. A regional model (WRF/chem, http://ruc.fsl.noaa.gov/wrf/WG11/) is employed to determine what fraction of β-pinene emitted reacts with NO$_3$ vs. O$_3$ and OH over a typical July night. The region is modeled with 4 km horizontal resolution and 1 h temporal resolution, using North American Regional Reanalysis (NARR) meteorological data. The US EPA's

1999 National Emissions Inventory (NEI-99, version 3) at 4 km horizontal resolution is used for anthropogenic emissions, while biogenic emissions are calculated online using the WRF/chem supplied emission module based on the description of Guenther et al. (1995), Simpson et al. (1995) and Richter et al. (1998). The module treats the emissions of isoprene, monoterpenes, other biogenic VOC (OVOC), and nitrogen emission by soil. Chemistry is modeled online using the RADM2 mechanism, for which the emissions of monoterpenes and OVOC are disaggregated into the lumped species, with β-pinene emissions added into "olt", the terminal olefin species class.

In every surface grid box, the fraction of "olt" (as a proxy for β-pinene) reacting with NO$_3$ is calculated by comparison of instantaneous oxidation rates for each hour of the night:

$$f_{NO_3} = \frac{k_{NO_3\text{-bpin}} \times [NO_3] \times [\text{olt}]}{k_{NO_3\text{-bpin}} \times [NO_3] \times [\text{olt}] + k_{O_3\text{-bpin}} \times [O_3] \times [\text{olt}] + k_{OH\text{-bpin}} \times [OH] \times [\text{olt}]} \quad (8)$$

Averaged over the California domain, f_{NO_3} is observed to be 0.75±0.03 over the course of 3 modeled nights in July 2000. Applying this factor and the observed 50% SOA mass yield from NO$_3$+β-pinene to the nighttime β-pinene emissions estimate, we arrive at a regional nighttime NO$_3$-β-pinene SOA source estimate of 1.7 tons hr^{-1}.

The model average nighttime lifetime of β-pinene is ~5–6 h, and daytime lifetime ~1–3 h. Based on these lifetimes and the diurnal cycle of monoterpene emissions (Sakulyanontvittaya et al., 2008), afternoon-emitted β-pinene that survives past sundown would add to this source estimate by of order 30%. The source estimate could be further increased by daytime NO$_3$ oxidation of β-pinene within forest canopies, which according to some models (Forkel et al., 2006; Fuentes et al., 2007) contributes up to 50% of daytime oxidation of monoterpenes. On the other hand, these models predict a fine scale vertical structure at night that is not captured by the WRF model, in which the lowest grid box has a height of 46 m. This (presently unquantifiable) effect could increase or decrease the nighttime source estimate.

Another recent model study (Russell and Allen, 2005) found that NO$_3$+β-pinene is a significant (~15% of monoterpenes + aromatic derived SOA) contributor to SOA formation in the Houston, Texas area, with an August daily formation rate of 587–975 kg day^{-1}, or 0.44–0.72 tons hr^{-1}, in an area of 16 km^2 around the urban center. The comparison of this Houston source with our total California (4.1×10^5 km^2) estimate of 1.7 tons hr^{-1} seems reasonable, since the latter includes the outflow of multiple urban areas. In California, maximum modeled [NO$_3$]×[olt] (β-pinene proxy) is observed in the mountains downwind of Sacramento, the San Francisco Bay area, and Los Angeles.

We can put this California SOA source estimate of 1.7 tons hr^{-1} into regional context by comparing

to fine particulate matter (PM$_{2.5}$) emissions for California. The California Air Resources Board estimated statewide annual average PM$_{2.5}$ emissions for 2006 of 1054 tons day^{-1}=44 tons hr^{-1}(CARB California Emissions Forecasting System, http://www.arb.ca.gov/app/emsinv/fcemssumcat2006.php). Hence, regional SOA production from this single monoterpene-oxidant system is estimated to be ~4% of inventoried total California fine particulate emissions. Recall that β-pinene accounts for only one quarter of total monoterpenes emissions. Hence, if all monoterpene SOA yields are similar to β-pinene (a gross approximation, as there have been very few measurements of these yields), the source estimate from NO$_3$ + monoterpenes would be ~16% of estimated total California PM$_{2.5}$ emissions. These calculations assume that the regional estimate made here is robust despite the caveats mentioned above, and that the state inventory of PM$_{2.5}$ accurately includes all anthropogenic and biogenic organic emissions, both of which introduce significant uncertainty to the relative importance of this SOA source regionally. We emphasize again that this estimate relies on our measured NO$_3$ + β-pinene SOA mass yield of 50%, which may or may not be representative of other monoterpenes. Nevertheless, this calculation clearly shows the need for better quantification of the NO$_3$ + monoterpene SOA source.

Global annual emissions of β-pinene are ~30 Tg C year^{-1} out of total biogenic emissions estimated at 1150 Tg C year^{-1} (Griffin et al., 1999b; Guenther et al., 1995). Isoprene makes up a large fraction of global biogenic emissions, predicted to be 389 Tg C year^{-1} by Ng et al. (2008) using the MEGAN model (Guenther et al., 2006). Ng et al. estimated an SOA source of 2–3 Tg year^{-1} from NO$_3$ + isoprene, using the GEOS-Chem global model and an average of their laboratory measured SOA mass yield of 10% (Ng et al., 2008). If we assume that the spatial overlap of biogenic isoprene and β-pinene emissions with regions of high NO$_x$ are similar, we can scale this NO$_3$ + isoprene source estimate by the ratios of total emissions of the biogenic precursors and SOA yields to arrive at a crude global SOA source estimate for NO$_3$+β-pinene. This assumption of similar overlap with NO$_x$ seems roughly appropriate given the spatial patterns of isoprene and monoterpenes emissions (Guenther et al., 1995). It appears that this estimate will, if anything, underestimate the monoterpenes-derived SOA source, as those emissions exhibit broader spatial extent, especially in the Northern Hemisphere summer. The result of this scaling of the Ng et al. (2008) isoprene source estimate gives a global SOA source of (2–3×(0.5/0.1)×(30/389)=) 0.8–1.2 Tg year^{-1} from NO$_3$+β-pinene.

A recent estimate of global mean monoterpene-derived SOA source was 7 Tg year^{-1} (Goto et al., 2008), while an earlier study estimated a total biogenic-derived SOA source of 18.5 Tg yr^{-1} (Griffin et al., 1999b). Goto et al. (2008) used a partitioning equilibrium constant (proportional to aerosol concentration/gas concentration) for

NO_3-monoterpene products that is an order of magnitude smaller than that for OH products and a factor of 6 smaller than for O_3 products, based on measurements of α-pinene partitioning (Griffin et al., 1999a). This same observational data led Griffin et al. (1999b) to neglect NO_3-oxidation from their (significantly higher) estimate of biogenic-derived SOA. The global estimate derived here of 0.8–1.2 Tg year^{-1} SOA from the *single* oxidant/monoterpene system of $NO_3+\beta$-pinene, in conjunction with reports of global models underpredicting SOA loading measured in field campaigns by up to 2 orders of magnitude (Heald et al., 2005; Volkamer et al., 2006), suggests that these NO_3 oxidation sources may be a significant missing source of organic aerosol in current models.

If we again scale this SOA source estimate by a factor of 4 to obtain an estimate for all monoterpenes (assuming SOA yield is similar), we arrive at a global SOA source from NO_3 + monoterpenes of 3.2–4.8 Tg year^{-1}. This can be compared to two recent estimates of *total* global mean SOA source, which vary from 12–70 Tg year^{-1} (Kanakidou et al., 2005) to 140–910 Tg year^{-1} (Goldstein and Galbally, 2007). The results presented here suggest that NO_3 + monoterpenes are responsible for of order 5 Tg year^{-1} of SOA, making them about 8% of the highest value reported by Kanakidou et al. (2005) and 0.5%–3% of the aerosol source suggested by Goldstein and Galbally. These fractions suggest that a NO_3 secondary organic aerosol source cannot be neglected.

4 Conclusions

Environmental chamber measurements of SOA formation in the reaction of $NO_3+\beta$-pinene are reported for dry and humid (60% RH) conditions with no seed aerosol. A gas-phase kinetics model with absorptive gas/aerosol partitioning reproduces the observed concentration time traces. Humidity below 60% RH does not appear to affect SOA formation appreciably; the mass yield of aerosol is ~50% under both dry and 60% RH conditions. In both cases, SOA formation is correlated with organic nitrate formation, which accounts for 40–45% of the β-pinene loss. The vapor pressure of the condensing organic nitrate in the absorptive gas/aerosol partitioning model is estimated to be 4–5×10^{-6} Torr (5–7×10^{-4} Pa). Organic nitrates also appear in the aerosol at very early times and therefore appear to be involved in nucleation as well.

The ratio of $NO_2^+:NO^+$ measured by the AMS in these experiments is significantly lower than for inorganic nitrate salts. This allows unambiguous assignment of the aerosol nitrate as deriving from organic nitrates. The observation of several organic fragments correlated with nitrate suggests some elements of the chemical formula of the nitrates. This distinct fractionation pattern could be used to identify organic nitrates in ambient data.

Based on estimated vapor pressures, AMS mass spectra, and AMS organic to nitrate ratio at low vaporizer temper-

ature, mono- and di-hydroxynitrates are proposed as structures of the aerosol organic nitrate. These organic nitrates constitute only 32–41% of the total aerosol mass, indicating that significant co-condensation of pure organic molecules must occur. The identity of these organic species is unknown. A nopinone-derived oligomer is proposed as one possibility.

Based on regional and global emissions of monoterpenes and estimates of relative rates of reaction with NO_3 and other oxidants, the ~50% mass yield of SOA from $NO_3+\beta$-pinene observed here translates to a significant regional and global SOA source. Because β-pinene constitutes only 25% of monoterpene emissions and only 3% of total biogenic hydrocarbon emissions, this suggests that the oxidation of biogenic VOCs contributes significantly to global secondary organic aerosol loading.

Edited by: M. Kulmala

References

SAPHIR homepage: http://www.fz-juelich.de/icg/icg-2/saphir/, last access: 18 February 2009.

Aldener, M., Brown, S. S., Stark, H., Williams, E. J., Lerner, B. M., Kuster, W. C., Goldan, P. D., Quinn, P. K., Bates, T. S., Fehsenfeld, F. C., and Ravishankara, A. R.: Reactivity and loss mechanisms of NO_3 and N_2O_5 in a polluted marine environment: Results from in situ measurements during New England Air Quality Study 2002, J. Geophys. Res.-Atmos., 111, D23S73, doi:10.1029/2006JD007252, 2006.

Alfaro-Moreno, E., Nawrot, T. S., Nemmar, A., and Nemery, B.: Particulate matter in the environment: pulmonary and cardiovascular effects, Curr. Opin. Pulm. Med., 13, 98–106, 2007.

Alfarra, M. R., Paulsen, D., Gysel, M., Garforth, A. A., Dommen, J., Prévôt, A. S. H., Worsnop, D. R., Baltensperger, U., and Coe, H.: A mass spectrometric study of secondary organic aerosols formed from the photooxidation of anthropogenic and biogenic precursors in a reaction chamber, Atmos. Chem. Phys., 6, 5279–5293, 2006,
http://www.atmos-chem-phys.net/6/5279/2006/.

Allan, J. D., Delia, A. E., Coe, H., Bower, K. N., Alfarra, M. R., Jimenez, J. L., Middlebrook, A. M., Drewnick, F., Onasch, T. B., Canagaratna, M. R., Jayne, J. T., and Worsnopf, D. R.: A generalised method for the extraction of chemically resolved mass spectra from aerodyne aerosol mass spectrometer data, J. Aerosol Sci., 35, 909—922, 2004.

Apel, E. C., Brauers, T., Koppmann, R., Bandowe, B., Bossmeyer, J., Holzke, C., Tillmann, R., Wahner, A., Wegener, R., Brunner,

A., Jocher, M., Ruuskanen, C., Spirig, C., Steigner, R., Stein-brecher, R., Gomez Alvarez, E., Mueller, K., Burrows, J. P., Schade, G., Solomon, S. J., Ladstaetter-Weissenmayer, A., Simmonds, P., Young, D., Hopkins, J. R., Lewis, A. C., Legreid, G., Reimann, S., Hansel, A., Wisthaler, A., Blake, R. S., Ellis, A. M., Monks, P. S., and Wyche, K. P.: Intercomparison of oxygenated volatile organic compound (OVOC) measurements at the SAPHIR atmosphere simulation chamber, J. Geophys. Res.-Atmos., in press, 2009.

Apodaca, R. L., Simpson, W. R., Ball, S. M., Brauers, T., Brown, S. S., Cohen, R. C., Crowley, J., Dorn, H.-P., Dubé, W. P., Fry, J. L., Fuchs, H., Haseler, R., Heitmann, U., Kato, S., Kajii, Y., Kiendler-Scharr, A., Kleffmann, J., Labazan, I., Matsumoto, J., Nishida, S., Rollins, A. W., Tillmann, R., Wahner, A., Wegener, R., and Wooldridge, P. J.: Intercomparison of N$_2$O$_5$ sensors using SAPHIR reaction chamber, Atmos. Chem. Phys., in preparation, 2009.

Atkinson, R.: Gas-phase tropospheric chemistry of volatile organic compounds, 1. Alkanes and alkenes, J. Phys. Chem. Ref. Data, 26, 215–290, 1997.

Barnes, I., Bastian, V., Becker, K. H., and Tong, Z.: Kinetics and Products of the Reactions of NO$_3$ with Monoalkenes, Dialkenes, and Monoterpenes, J. Phys. Chem., 94, 2413–2419, 1990.

Berndt, T. and Boge, O.: Products and mechanism of the gas-phase reaction of NO$_3$ radicals with a-pinene, J. Chem. Soc. Faraday T., 93, 3021–3027, 1997.

Bohn, B., Rohrer, F., Brauers, T., and Wahner, A.: Actinometric measurements of NO$_2$ photolysis frequencies in the atmosphere simulation chamber SAPHIR, Atmos. Chem. Phys., 5, 493–503, 2005,
http://www.atmos-chem-phys.net/5/493/2005/.

Bonn, B. and Moorgat, G. K.: New particle formation during a- and b-pinene oxidation by O$_3$, OH and NO$_3$, and the influence of water vapour: particle size distribution studies, Atmos. Chem. Phys., 2, 183–196, 2002,
http://www.atmos-chem-phys.net/2/183/2002/.

Bossmeyer, J., Brauers, T., Richter, C., Rohrer, F., Wegener, R., and Wahner, A.: Simulation chamber studies on the NO$_3$ chemistry of atmospheric aldehydes, Geophys. Res. Lett., 33, L18810, doi:10.1029/2006GL026778, 2006.

Brauers, T., Bossmeyer, J., Dorn, H.-P., Schlosser, E., Tillmann, R., Wegener, R., and Wahner, A.: Investigation of the formaldehyde differential absorption cross section at high and low spectral resolution in the simulation chamber SAPHIR, Atmos. Chem. Phys., 7, 3579–3586, 2007,
http://www.atmos-chem-phys.net/7/3579/2007/.

Burkholder, J. B., Baynard, T., Ravishankara, A. R., and Lovejoy, E. R.: Particle nucleation following the O$_3$ and OH initiated oxidation of alpha-pinene and beta-pinene between 278 and 320 K, J. Geophys. Res.-Atmos., 112, D10216, doi:10.1029/2006JD007783, 2007.

Calvert, J. G., Atkinson, J. A., Kerr, J. A., Madronich, S., Moortgat, G. K., Wallington, T. J., and Yarwood, G.: Mechanisms of the atmospheric oxidation of the alkenes, Oxford University Press, New York, NY, 2000.

Canagaratna, M. R., Jayne, J. T., Jimenez, J. L., Allan, J. D., Alfarra, M. R., Zhang, Q., Onasch, T. B., Drewnick, F., Coe, H., Middlebrook, A., Delia, A., Williams, L. R., Trimborn, A. M., Northway, M. J., DeCarlo, P. F., Kolb, C. E., Davidovits, P., and

Worsnop, D. R.: Chemical and microphysical characterization of ambient aerosols with the aerodyne aerosol mass spectrometer, Mass Spectrom. Rev., 26, 185–222, 2007.

Capouet, M. and Müller, J.-F.: A group contribution method for estimating the vapour pressures of α-pinene oxidation products, Atmos. Chem. Phys., 6, 1455–1467, 2006,
http://www.atmos-chem-phys.net/6/1455/2006/.

Capouet, M., Müller, J. F., Ceulemans, K., Compernolle, S., Vereecken, L., and Peeters, J.: Modeling aerosol formation in alpha-pinene photo-oxidation experiments, J. Geophys. Res.-Atmos., 113, D02308, doi:10.1029/2007JD008995, 2008.

Cottrell, L. D., Griffin, R. J., Jimenez, J. L., Zhang, Q., Ulbrich, I., Ziemba, L. D., Beckman, P. J., Sive, B. C., and Talbot, R. W.: Submicron particles at Thompson Farm during ICARTT measured using aerosol mass spectrometry, J. Geophys. Res.-Atmos., 113, D08212, doi:10.1029/2007JD009192, 2008.

Cowie, J. M. G.: Polymers: Chemistry and physics of modern materials, 2nd ed., Blackie Academic & Professional, Glasgow, UK, 28 pp., 1991.

Day, D. A., Wooldridge, P. J., Dillon, M. B., Thornton, J. A., and Cohen, R. C.: A thermal dissociation laser-induced fluorescence instrument for in situ detection of NO$_2$, peroxy nitrates, alkyl nitrates, and HNO$_3$, J. Geophys. Res.-Atmos., 107(D5–6), 4046, doi:10.1029/2001JD000779, 2002.

de Gouw, J. A., Middlebrook, A. M., Warneke, C., Goldan, P. D., Kuster, W. C., Roberts, J. M., Fehsenfeld, F. C., Worsnop, D. R., Canagaratna, M. R., Pszenny, A. A. P., Keene, W. C., Marchewka, M., Bertman, S. B., and Bates, T. S.: Budget of organic carbon in a polluted atmosphere: Results from the New England Air Quality Study in 2002, J. Geophys. Res.-Atmos., 110, D16305, doi:10.1029/2004JD005623, 2005.

DeCarlo, P. F., Slowik, J. G., Worsnop, D. R., Davidovits, P., and Jimenez, J. L.: Particle morphology and density characterization by combined mobility and aerodynamic diameter measurements. Part 1: Theory, Aerosol Sci. Tech., 38, 1185–1205, 2004.

Docherty, K. S. and Ziemann, P. J.: Effects of stabilized Criegee intermediate and OH radical scavengers on aerosol formation from reactions of β-pinene with O$_3$, Aerosol Sci. Tech., 37, 877–891, 2003.

Dockery, D. W. and Pope, C. A.: Acute Respiratory Effects of Particulate Air-Pollution, Annu. Rev. Publ. Health, 15, 107–132, 1994.

Dorn, H. P., Apodaca, R. L., Ball, S. M., Brauers, T., Brown, S. S., Cohen, R. C., Crowley, J., Dubé, W. P., Fry, J. L., Fuchs, H., Haseler, R., Heitmann, U., Jones, R., Kato, S., Kajii, Y., Kiendler-Scharr, A., Labazan, I., Matsumoto, J., Meinen, J., Nishida, S., Platt, U., Rohrer, F., Rollins, A.W., Ruth, A. A., Schlosser, E., Schuster, G., Shillings, A., Simpson, W., Thieser, J., Tillmann, R., Varma, R., Venables, D., Wahner, A., Wegener, R., and Wooldridge, P. J.: Intercomparison of NO$_3$ measurement techniques at the simulation chamber SAPHIR, Atmos. Chem. Phys., in preparation, 2009.

Dubé, W. P., Brown, S. S., Osthoff, H. D., Nunley, M. R., Ciciora, S. J., Paris, M. W., McLaughlin, R. J., and Ravishankara, A. R.: Aircraft instrument for simultaneous, in situ measurement of NO$_3$ and N$_2$O$_5$ via pulsed cavity ring-down spectroscopy, Rev. Sci. Instrum., 77, 034101, doi:10.1063/1.2176058, 2006.

Dubowski, Y., Sumner, A. L., Menke, E. J., Gaspar, D. J., Newberg, J. T., Hoffman, R. C., Penner, R. M., Hemminger, J. C., and

Finlayson-Pitts, B. J.: Interactions of gaseous nitric acid with surfaces of environmental interest, Phys. Chem. Chem. Phys., 6, 3879–3888, 2004.

Farmer, D. K., Cohen, R. C., Perring, A. E., Wooldridge, P. J., Blake, D., Baker, A., Huey, L. G., Sjostedt, S., Tanner, D., Vargas, O., de Gouw, J., Warneke, C., Kuster, W., Murphy, J. G.: NO_y partitioning and the role of alkyl nitrates in air quality in the Mexico City Area, Atmos. Chem. Phys., in preparation, 2009.

Forkel, R., Klemm, O., Graus, M., Rappengluck, B., Stockwell, W. R., Grabmer, W., Held, A., Hansel, A., and Steinbrecher, R.: Trace gas exchange and gas phase chemistry in a Norway spruce forest: a study with a coupled 1-dimensional canopy atmospheric chemistry emission model, Atmos. Environ., 40, 28–42, 2006.

Forster, P., Ramaswamy, V., Artaxo, P., Berntsen, T., Betts, R., Fahey, D. W., Haywood, J., Lean, J., Lowe, D. C., Myhre, G., Nganga, J., Prinn, R., Raga, G., Schulz, M., and Van Dorland, R.: Changes in Atmospheric Constitutents and in Radiative Forcing, in: Climate Change 2007: The Physical Science Basis. Contribution fo Working Group I to the Fourth Assessment Report of the Intergovernmental Panel on Climate Change, edited by: Solomon, S., Qin, D., Manning, M., Chen, Z., Marquis, M., Averyt, K. B., Tignor, M., and Miller, H. L., Cambridge University Press, Cambridge, United Kingdom and New York, NY, USA, 2007.

Fountoukis, C., Nenes, A., Sullivan, A., Weber, R., VanReken, T., Fischer, M., Matías, E., Moya, M., Farmer, D., and Cohen, R. C.: Thermodynamic characterization of Mexico City aerosol during MILAGRO 2006, Atmos. Chem. Phys. Discuss., 7, 9203–9233, 2007,
http://www.atmos-chem-phys-discuss.net/7/9203/2007/.

Fuchs, H. Brown, S. S., Dubé, W., et al.: Intercomparison of instruments measuring NO_2 at the atmosphere simulation chamber SAPHIR, Atmos. Chem. Phys., in preparation, 2009.

Fuentes, J. D., Wang, D., Bowling, D. R., Potosnak, M., Monson, R. K., Goliff, W. S., and Stockwell, W. R.: Biogenic hydrocarbon chemistry within and above a mixed deciduous forest, J. Atmos. Chem., 56, 165–185, 2007.

Fuzzi, S., Andreae, M. O., Huebert, B. J., Kulmala, M., Bond, T. C., Boy, M., Doherty, S. J., Guenther, A., Kanakidou, M., Kawamura, K., Kerminen, V.-M., Lohmann, U., Russell, L. M., and Pöschl, U.: Critical assessment of the current state of scientific knowledge, terminology, and research needs concerning the role of organic aerosols in the atmosphere, climate, and global change, Atmos. Chem. Phys., 6, 2017–2038, 2006,
http://www.atmos-chem-phys.net/6/2017/2006/.

Geyer, A., Alicke, B., Konrad, S., Schmitz, T., Stutz, J., and Platt, U.: Chemistry and oxidation capacity of the nitrate radical in the continental boundary layer near Berlin, J. Geophys. Res.-Atmos., 106, 8013–8025, 2001.

Geyer, A., Alicke, B., Ackermann, R., Martinez, M., Harder, H., Brune, W., di Carlo, P., Williams, E., Jobson, T., Hall, S., Shetter, R., and Stutz, J.: Direct observations of daytime NO_3: Implications for urban boundary layer chemistry, J. Geophys. Res.-Atmos., 108(D12), 4268, doi:10.1029/2002JD002967, 2003.

Goldstein, A. H. and Galbally, I. E.: Known and unexplored organic constituents in the earth's atmosphere, Environ. Sci. Technol., 41, 1514–1521, 2007.

Gong, H. M., Matsunaga, A., and Ziemann, P. J.: Products and mechanism of secondary organic aerosol formation from reac-

tions of linear alkenes with NO_3 radicals, J. Phys. Chem. A, 109, 4312–4324, 2005.

Goto, D., Takemura, T., and Nakajima, T.: Importance of global aerosol modeling including secondary organic aerosol formed from monoterpene, J. Geophys. Res.-Atmos., 113, D07205, doi:10.1029/2007JD009019, 2008.

Griffin, R. J., Cocker, D. R., Flagan, R. C., and Seinfeld, J. H.: Organic aerosol formation from the oxidation of biogenic hydrocarbons, J. Geophys. Res.-Atmos., 104, 3555–3567, 1999a.

Griffin, R. J., Cocker, D. R., Seinfeld, J. H., and Dabdub, D.: Estimate of global atmospheric organic aerosol from oxidation of biogenic hydrocarbons, Geophys. Res. Lett., 26, 2721–2724, 1999b.

Guenther, A., Hewitt, C. N., Erickson, D., Fall, R., Geron, C., Graedel, T., Harley, P., Klinger, L., Lerdau, M., McKay, W. A., Pierce, T., Scholes, B., Steinbrecher, R., Tallamraju, R., Taylor, J., and Zimmerman, P.: A Global-Model of Natural Volatile Organic-Compound Emissions, J. Geophys. Res.-Atmos., 100, 8873–8892, 1995.

Guenther, A., Karl, T., Harley, P., Wiedinmyer, C., Palmer, P. I., and Geron, C.: Estimates of global terrestrial isoprene emissions using MEGAN (Model of Emissions of Gases and Aerosols from Nature), Atmos. Chem. Phys., 6, 3181–3210, 2006,
http://www.atmos-chem-phys.net/6/3181/2006/.

Hallquist, M., Wangberg, I., Ljungstrom, E., Barnes, I., and Becker, K. H.: Aerosol and product yields from NO_3 radical-initiated oxidation of selected monoterpenes, Environ. Sci. Technol., 33, 553–559, 1999.

Hanke, M., Uecker, J., Reiner, T., and Arnold, F.: Atmospheric peroxy radicals: ROXMAS, a new mass-spectrometric methodology for speciated measurements of HO_2 and ΣRO_2 and first results, Int. J. Mass Spec., 213, 91–99, 2002.

Heald, C. L., Jacob, D. J., Park, R. J., Russell, L. M., Huebert, B. J., Seinfeld, J. H., Liao, H., and Weber, R. J.: A large organic aerosol source in the free troposphere missing from current models, Geophys. Res. Lett., 32, L18809, doi:10.1029/2005GL023831, 2005.

Hoffmann, T., Odum, J. R., Bowman, F., Collins, D., Klockow, D., Flagan, R. C., and Seinfeld, J. H.: Formation of organic aerosols from the oxidation of biogenic hydrocarbons, J. Atmos. Chem., 26, 189–222, 1997.

Jay, K. and Stieglitz, L.: The Gas-Phase Addition of NOx to Olefins, Chemosphere, 19, 1939–1950, 1989.

Jenkin, M. E.: Modelling the formation and composition of secondary organic aerosol from α- and β-pinene ozonolysis using MCM v3, Atmos. Chem. Phys., 4, 1741–1757, 2004,
http://www.atmos-chem-phys.net/4/1741/2004/.

Kamens, R., Jang, M., Chien, C. J., and Leach, K.: Aerosol formation from the reaction of alpha-pinene and ozone using a gasphase kinetics aerosol partitioning model, Environ. Sci. Technol., 33, 1430–1438, 1999.

Kanakidou, M., Seinfeld, J. H., Pandis, S. N., Barnes, I., Dentener, F. J., Facchini, M. C., Van Dingenen, R., Ervens, B., Nenes, A., Nielsen, C. J., Swietlicki, E., Putaud, J. P., Balkanski, Y., Fuzzi, S., Horth, J., Moortgat, G. K., Winterhalter, R., Myhre, C. E. L., Tsigaridis, K., Vignati, E., Stephanou, E. G., and Wilson, J.: Organic aerosol and global climate modelling: a review, Atmos. Chem. Phys., 5, 1053–1123, 2005,
http://www.atmos-chem-phys.net/5/1053/2005/.

Korhonen, H., Lehtinen, K. E. J., and Kulmala, M.: Multicomponent aerosol dynamics model UHMA: model development and validation, Atmos. Chem. Phys., 4, 757–771, 2004, http://www.atmos-chem-phys.net/4/757/2004/.

Kurtenbach, R., Ackermann, R., Becker, K. H., Geyer, A., Gomes, J. A. G., Lorzer, J. C., Platt, U., and Wiesen, P.: Verification of the contribution of vehicular traffic to the total NMVOC emissions in Germany and the importance of the NO$_3$ chemistry in the city air, J. Atmos. Chem., 42, 395–411, 2002.

Lee, A., Goldstein, A. H., Keywood, M. D., Gao, S., Varutbangkul, V., Bahreini, R., Ng, N. L., Flagan, R. C., and Seinfeld, J. H.: Gas-phase products and secondary aerosol yields from the ozonolysis of ten different terpenes, J. Geophys. Res.-Atmos., 111, D07302, doi:10.1029/2005JD006437, 2006.

Lelieveld, J. and Crutzen, P. J.: The Role of Clouds in Tropospheric Photochemistry, J. Atmos. Chem., 12, 229–267, 1991.

Lindinger, W., Hansel, A., and Jordan, A.: On-line monitoring of volatile organic compounds at pptv levels by means of proton-transfer-reaction mass spectrometry (PTR-MS) – Medical applications, food control and environmental research, Int. J. Mass. Spectrom., 173, 191–241, 1998.

Moise, T., Talukdar, R. K., Frost, G. J., Fox, R. W., and Rudich, Y.: Reactive uptake of NO$_3$ by liquid and frozen organics, J. Geophys. Res., 107(D2), 4014, doi:10.1029/2001JD000334, 2002.

Moldanova, J. and Ljungstrom, E.: Modelling of particle formation from NO$_3$ oxidation of selected monoterpenes, J. Aerosol Sci., 31, 1317–1333, 2000.

Ng, N. L., Kwan, A. J., Surratt, J. D., Chan, A. W. H., Chhabra, P. S., Sorooshian, A., Pye, H. O. T., Crounse, J. D., Wennberg, P. O., Flagan, R. C., and Seinfeld, J. H.: Secondary organic aerosol (SOA) formation from reaction of isoprene with nitrate radicals (NO$_3$), Atmos. Chem. Phys., 8, 4117–4140, 2008, http://www.atmos-chem-phys.net/8/4117/2008/.

Odum, J. R., Hoffmann, T., Bowman, F., Collins, D., Flagan, R. C., and Seinfeld, J. H.: Gas/Particle Partitioning and Secondary Organic Aerosol Yields, Environ. Sci. Technol., 30, 2580–2585, 1996.

Pankow, J. F.: An Absorption-Model of Gas-Particle Partitioning of Organic-Compounds in the Atmosphere, Atmos. Environ., 28, 185–188, 1994a.

Pankow, J. F.: An Absorption-Model of the Gas Aerosol Partitioning Involved in the Formation of Secondary Organic Aerosol, Atmos. Environ., 28, 189–193, 1994b.

Poling, B. E., Prausnitz, J. M., and O'Connell, J. P.: The properties of gases and liquids, 5th ed., McGraw-Hill, New York, 2001.

Pope, C. A., Dockery, D. W., and Schwartz, J.: Review of Epidemiological Evidence of Health-Effects of Particulate Air-Pollution, Inhal. Toxicol., 7, 1–18, 1995.

Pope, C. A.: Mortality effects of longer term exposures to fine particulate air pollution: Review of recent epidemiological evidence, Inhal. Toxicol., 19, 33–38, 2007.

Quinn, P. K., Bates, T. S., Coffman, D., Onasch, T. B., Worsnop, D., Baynard, T., de Gouw, J. A., Goldan, P. D., Kuster, W. C., Williams, E., Roberts, J. M., Lerner, B., Stohl, A., Pettersson, A., and Lovejoy, E. R.: Impacts of sources and aging on submicrometer aerosol properties in the marine boundary layer across the Gulf of Maine, J. Geophys. Res.-Atmos., 111, D23S36, doi:10.1029/2006JD007582, 2006.

Richter, K., Knoche, R., Schoenemeyer, T., Smiatek, G., and

Steinbrecher, R.: Estimate of biogenic hydrocarbon emissions, Umweltwissenschaften und Schadstoff-Forschung, 10, 319–325, 1998.

Rohrer, F., Bohn, B., Brauers, T., Brüning, D., Johnen, F.-J., Wahner, A., and Kleffmann, J.: Characterisation of the photolytic HONO-source in the atmosphere simulation chamber SAPHIR, Atmos. Chem. Phys., 5, 2189–2201, 2005, http://www.atmos-chem-phys.net/5/2189/2005/.

Russell, M. and Allen, D. T.: Predicting secondary organic aerosol formation rates in southeast Texas, J. Geophys. Res.-Atmos., 110, D07S17, doi:10.1029/2004JD004722, 2005.

Sakulyanontvittaya, T., Duhl, T., Wiedinmyer, C., Helmig, D., Matsunaga, S., Potosnak, M., Milford, J., and Guenther, A.: Monoterpene and Sesquiterpene Emission Estimates for the United States, Environ. Sci. Technol., 42, 1623–1629, 2008.

Sander, S. P., Golden, D. M., Kurylo, M. J., Moortgat, G. K., Wine, P. H., Ravishankara, A. R., Kolb, C. E., Molina, M. J., Finlayson-Pitts, B. J., Huie, R. E., Orkin, V. L., Friedl, R. R., and Keller-Rudek, H.: Chemical kinetics and photochemical data for use in atmospheric studies: evaluation number 15, Jet Propulsion Laboratory, California Institute of Technology, Pasadena, CA, 2006.

Saunders, S. M., Jenkin, M. E., Derwent, R. G., and Pilling, M. J.: Protocol for the development of the Master Chemical Mechanism, MCM v3 (Part A): tropospheric degradation of non-aromatic volatile organic compounds, Atmos. Chem. Phys., 3, 161–180, 2003, http://www.atmos-chem-phys.net/3/161/2003/.

Schichtel, B. A., Malm, W. C., Bench, G., Fallon, S., McDade, C. E., Chow, J. C., and Watson, J. G.: Fossil and contemporary fine particulate carbon fractions at 12 rural and urban sites in the United States, J. Geophys. Res.-Atmos., 113, D02311, doi:10.1029/2007JD008605, 2008.

Scott, K. I. and Benjamin, M. T.: Development of a biogenic volatile organic compounds emission inventory for the SCOS97-NARSTO domain, Atmos. Environ., 37, 39–49, 2003.

Seinfeld, J. H. and Pankow, J. F.: Organic Atmospheric Particulate Material, Annu. Rev. Phys. Chem., 54, 121–140, doi:10.1146/annurev.physchem.54.011002.103756, 2003.

Simpson, D., Guenther, A., Hewitt, C. N., and Steinbrecher, R.: Biogenic Emissions in Europe. 1. Estimates and Uncertainties, J. Geophys. Res.-Atmos., 100, 22875–22890, 1995.

Spittler, M., Barnes, I., Bejan, I., Brockmann, K. J., Benter, T., and Wirtz, K.: Reactions of NO$_3$ radicals with limonene and alpha-pinene: Product and SOA formation, Atmos. Environ., 40, S116–S127, 2006.

Thornton, J. A., Wooldridge, P. J., and Cohen, R. C.: Atmospheric NO$_2$: In situ laser-induced fluorescence detection at parts per trillion mixing ratios, Anal. Chem., 72, 528–539, 2000.

TSI, I.: Aerosol Instrument Manager Software for SMPS Spectrometer User's Manual P/N 1930038 Revision G, October, 2007.

Turpin, B. J. and Huntzicker, J. J.: Identification of Secondary Organic Aerosol Episodes and Quantitation of Primary and Secondary Organic Aerosol Concentrations During SCAQS, Atmos. Environ., 29, 3527–3544, 1995.

Verheggen, B. and Mozurkewich, M.: An inverse modeling procedure to determine particle growth and nucleation rates from measured aerosol size distributions, Atmos. Chem. Phys., 6, 2927–2942, 2006, http://www.atmos-chem-phys.net/6/2927/2006/.

Volkamer, R., Jimenez, J. L., San Martini, F., Dzepina, K., Zhang, Q., Salcedo, D., Molina, L. T., Worsnop, D. R., and Molina, M. J.: Secondary organic aerosol formation from anthropogenic air pollution: Rapid and higher than expected, Geophys. Res. Lett., 33, L17811, doi:10.1029/2006GL026899, 2006.

Wangberg, I., Barnes, I., and Becker, K. H.: Product and mechanistic study of the reaction of NO$_3$ radicals with alpha-pinene, Environ. Sci. Technol., 31, 2130–2135, 1997.

Weber, R. J., Sullivan, A. P., Peltier, R. E., Russell, A., Yan, B., Zheng, M., de Gouw, J., Warneke, C., Brock, C., Holloway, J. S., Atlas, E. L., and Edgerton, E.: A study of secondary organic aerosol formation in the anthropogenic-influenced southeastern United States, J. Geophys. Res.-Atmos., 112, D13302, doi:10.1029/2007JD008408, 2007.

Wegener, R., Brauers, T., Koppmann, R., Bares, S. R., Rohrer, F., Tillmann, R., Wahner, A., Hansel, A., and Wisthaler, A.: Simulation chamber investigation of the reactions of ozone with short-chained alkenes, J. Geophys. Res.-Atmos., 112, D13301, doi:10.1029/2006JD007531, 2007.

Winer, A. M., Atkinson, R., and Pitts, J. N.: Gaseous Nitrate Radical: Possible Nighttime Atmospheric Sink for Biogenic Organic Compounds, Science, 224, 156–159, 1984.

Winterhalter, R., Neeb, P., Grossmann, D., Kolloff, A., Horie, O., and Moortgat, G.: Products and Mechanism of the Gas Phase Reaction of Ozone with β–Pinene, J. Atmos. Chem., 35, 165–197, 2000.

Zhang, Q., Jimenez, J. L., Canagaratna, M. R., Allan, J. D., Coe, H., Ulbrich, I., Alfarra, M. R., Takami, A., Middlebrook, A. M., Sun, Y. L., Dzepina, K., Dunlea, E., Docherty, K., De-Carlo, P. F., Salcedo, D., Onasch, T., Jayne, J. T., Miyoshi, T., Shimono, A., Hatakeyama, S., Takegawa, N., Kondo, Y., Schneider, J., Drewnick, F., Borrmann, S., Weimer, S., Demerjian, K., Williams, P., Bower, K., Bahreini, R., Cottrell, L., Griffin, R. J., Rautiainen, J., Sun, J. Y., Zhang, Y. M., and Worsnop, D. R.: Ubiquity and dominance of oxygenated species in organic aerosols in anthropogenically-influenced Northern Hemisphere midlatitudes, Geophys. Res. Lett., 34, L13801, doi:10.1029/2007GL029979, 2007.